2018

Study of Seasonal change and Water Stress Condition in Plant Leaf Using Polarimetric Lidar Measurement

Prabeen Kattel
South Dakota State University

STUDY OF SEASONAL CHANGE AND WATER STRESS CONDITION IN PLANT LEAF USING POLARIMETRIC LIDAR MEASUREMENT

BY

PRABEEN KATTEL

A thesis submitted in partial fulfillment of the requirement of the

Master of Science

Major in Electrical Engineering

South Dakota State University

2018

STUDY OF SEASONAL CHANGE AND WATER STRESS CONDITION IN PLANT LEAF USING POLARIMETRIC LIDAR MEASUREMENT

PRABEEN KATTEL

This thesis is approved as a creditable and independent investigation by a candidate for the Master of Science degree and is acceptable for meeting the thesis requirements for this degree. Acceptance of this thesis does not imply that the conclusions reached by the candidate are necessarily the conclusions of the major department.

Songxin Tan, Ph.D. Date

Thesis Advisor

George Hamer, Ph.D. Date

Acting Head, Electrical Engineering and

Computer Science

Dean, Graduate School Date

ACKNOWLEDGMENT

Firstly, I would like to thank my research advisor Dr. Songxin Tan, Associate Professor in the Department of Computer and Electrical Engineering, South Dakota State University. Without his continuous inspiration, guidance, and support, I would not have been able to accomplish this research goal at this point. His valuable time, as well as financial support for the part of this work, helped me in every way to succeed.

I am grateful to the Electrical Engineering and Computer Science department for providing the chance to flourish my knowledge with proper financial support. I would like to acknowledge Miss Erin Benson for her co-operation and help in the laboratory experiments.

Finally, I would like to dedicate this thesis to my Father and Mother for their never-ending, unconditional love and support to my dreams and interests. I am highly grateful to my brothers and their family for their support.

CONTENTS

ABBREVIATIONS

AIS	Airborne Imaging spectroscopy
ALPS	Airborne Laser Polarization Sensor
ASD	Analytical Spectral Devices
ASDF	Averaged Square Difference Function
AVIRIS	Airborne Visible/Infrared imaging spectrometer
CHM	Canopy Height Model
DTM	Digital terrain models
EOS	Earth Observation System
Er: YAG	Erbium-doped Yttrium aluminum garnet
FET	Field Effect Transistor
GaAlAs	Gallium Aluminum arsenide
GLAS	Geoscience Laser Altimeter System
ICESAT	Ice, Cloud, and land Elevation Satellite
InGaAs	Indium Gallium Arsenide
IR	Infrared
LVIS	Laser vegetation imaging sensor
MAPL	Multiwavelength Airborne Polarimetric Lidar

MBLA	Multi-Beam laser altimeter
MSCL	Multispectral canopy lidar
Nd:YAG	Neodymium-doped Yttrium aluminum garnet
PIDAS	Portable Instant Display and Analysis spectrometer
POL-SAR	Polarimetric Synthetic Aperture Radar
PRF	Pulse repetition frequency
RADAR	Radio Detection and Ranging
RJMCMC	Reversible jump Markov chain Carlo
SAL	Synthetic Aperture Lidar
SAR	Synthetic Aperture Radar
SI	Separability index
Si-APD	Silicon Avalanche Photodiode
SLA	Shuttle Laser Altimeter
SLICER	Scanning lidar Imager of canopies By Echo Recovery
TOPSAT	Topography Satellite
UV	Ultraviolet
VCL	Vegetation canopy lidar

LIST OF FIGURES

LIST OF TABLES

ABSTRACT

STUDY OF SEASONAL CHANGE AND WATER STRESS CONDITION IN PLANT LEAF USING POLARIMETRIC LIDAR MEASUREMENT

PRABEEN KATTEL

2018

Study of vegetation is of great importance to the improvement of agriculture and forest management. Although there have been various attempts to characterize vegetation using remote sensing techniques, polarimetric lidar is a novel remote sensing tool that has shown potential in vegetation remote sensing. In this thesis, a near-infrared polarimetric lidar at 1064 nm was used to investigate the effects of seasonal change and water stress condition on plant leaves. Two variables, time and water content, affected the plant leaf laser depolarization ratio measurement. The first study focused on the maple tree in order to figure out how seasonal change affected the maple leaf depolarization. Seasonal trendline was obtained and revealed an overall downward trend over time. In the second study, the leaves from maple, lemon, and rubber trees were investigated to study the effect of water stress on the depolarization ratio. It was discovered that the leaf depolarization ratio increased for more water content and went down for less water content. In addition, leaf samples were collected in the morning, afternoon, and evening, respectively, to study the diurnal change. Statistical analysis suggested that depolarization ratio did not change significantly for the different times of a day. It was suggested that the seasonal change had a greater effect on depolarization than the diurnal change. This study demonstrates that the near-infrared polarimetric lidar system has an

ability to remotely characterize the vegetation internal conditions that may not be visible to the human eyes. Furthermore, the lidar system has the potential to differentiate the various plant species based on the depolarization ratio. In conclusion, the polarimetric lidar system at 1064-nm is an effective and sensitive enough remote sensing tool which can be widely used in active remote sensing.

CHAPTER 1 INTRODUCTION

1.1 Basic introduction of light

In the history of civilization, light is the very first hope of survival and existence. Ancient philosopher Aristotle believed that the essence of light is white light whereas colors are made up of a mixture of lightness and darkness[1]. In the 17th century, Sir Isaac Newton made a major discovery on the spectral decomposition of light as well as particle nature of the light[1]. When in 1690, Christiaan Huygens published a paper claiming the wave nature of light, he used wave nature of light to explain the reflection and refraction of light. During the interpretation of birefringence, Huygens made the discovery of polarization of light[2]. In 1807, Thomas Young demonstrated the interference fringe pattern for light coming from a single point of source and established the wave phenomenon of light[3]. In 1808, French engineer Etienne Louse Malus discovered a polarization of light by reflection[4]. Even though Malus did not interpret the phenomenon, he used the term polarization for the first time. Later in the nineteenth-century French physicist, Arago observed the polarization of light. From then, polarization phenomenon was on active research by various scientists. Scottish physicist James Clerk Maxwell in 1864 established four Maxwell's equations as the foundation of electromagnetism and the 'jewel of physics'. When Albert Einstein in 1905 announced the quantum nature of light, the greatest breakthrough in understanding the mystery of light happened. He stated that light is made up of particles called photons. Photons are discrete particles with their own energy level and frequency. He theoretically revealed the photoelectric effect of light based on the same quantum hypothesis for which he won Nobel prize in 1921.

1.2 Polarization of light

A light is an electromagnetic wave and electromagnetic wave is a transverse wave which contains both electric and magnetic field component. The vibrational planes of an electric and magnetic component of lights are numerous. The light with multiple vibrational planes is an unpolarized light. If the tip of the electric vector follows a linear plane, then it is linearly polarized light and if it follows an elliptical plane, it is called elliptically polarized light. The light produced by the sun or by candle flame is unpolarized light; but by several ways, light can be converted to be polarized. For example, unpolarized light can be converted to polarized light by passing it through the different medium. Reflected light from a nonmetallic surface causes some degree of polarization in the direction parallel to the surface. Light can be polarized by refraction and scattering too. Polarization causes the glare on the surface of the water. Fisherman wears polarized glass to remove the glare effect during the fishing. In nature, this polarization effect of light is of great importance. Even though a human cannot detect the polarization effect, many insects, birds, and fishes have the ability to sense the polarimetric change within the IR to UV spectrum[5]. Basically, there are four ways to do so: reflection, refraction, scattering, and transmission[6].

1.2.1 Polarization by polarizer

Polarizer consists of materials which are capable of blocking either vertical or horizontal plane of vibration of the electromagnetic wave. The polarizer can be thought as a long chain molecule that aligned within the filter in the same direction. During the filter fabrication, these molecules are stretched across the filter so that each molecule is aligned in one direction. Then when unpolarized light strikes the filter, the portion of wave

vibrating parallel to the alignment molecules are absorbed and perpendicular to the alignment of molecules are transmitted. That means the alignment of these molecules gives a polarization axis of the filter. Any vibrations that are perpendicular to the polarization axis are blocked by the filter.

1.2.2 Polarization by reflection

When the unpolarized light hit on the surface of any materials, reflected light may get polarized. This depends on the angle of incidence and types of material. Mainly nonmetallic surfaces give better polarization than metallic because metallic surface tends to reflect light with many different vibrational directions which are unpolarized. In the case when reflected and refracted light are perpendicular with each other, reflected light is completely polarized in the direction parallel to the plane of reflecting surfaces whereas refracted light is partially polarized.

1.2.3 Polarization by refraction

When light passes from one material to another material, at the surface of two material, the refracted light changes its path. This refracted light may acquire some degree of polarization, mostly in the plane perpendicular to the surface of the material.

1.2.4 Polarization by scattering

Polarization also occurs when the light is scattered traveling through a medium. When the light strikes an atom of the material, electrons in its atom get excited and causes the vibration. The vibrational mode of the molecules generates their own electromagnetic wave. When a newly generated wave strikes neighboring atom, those electrons are forced to generate some other electromagnetic waves with the frequency of the original wave. In

this way, vibrating electron produces electromagnetic waves radiative outward in various direction. This process causes the partial polarization of light.

1.3 What is remote sensing

Remote sensing is the technology and science which can detect, characterize and identify the object of interest without direct contact. It can observe the object's size, shape, location and other characteristics of an object from a far distance. Basically, in the system of remote sensing, reflected or radiated electromagnetic waves are received by the sensor at a far distance and this received wave carries the information of the object that reflects or radiates the wave. The sensor can be either active or passive. For example, sonar, radar, lidar are active sensors which send out their own source of illumination. Whereas some other passive sensors utilize either the radiation generated by re-emitted or reflected sunlight energy or self-radiated wave by the object. Example of the passive sensor includes spectrometer etc. Active remote sensing is less dependent on weather, and it has an ability to obtain the measurement day and night. It can examine the wave that is not sufficiently provided by the sunlight too. But this requires the generation of energy source to illuminate the target.

1.4 What is lidar technology

Lidar which is also referred to as LADAR or laser altimeter is an acronym for light detection and ranging. The technology consists of the laser source which emits an intense beam of the laser. This is a remote sensing technology on which laser beam travels a distance, hits the target, and comes back to the detector. The detected laser reflection can give a range, velocity, and other features of the target from which light gets reflected. The selection of laser wavelength is done based on the characteristics of the transmission

medium (absorption of atmosphere etc.), the target and its scattering property, requirements of the project, eye safety and the availability of laser and detector. Longer laser wavelength has lesser resolution than the shorter one. So, the wavelength is chosen based on the requirement. Lidar can be used in the range measurement purpose. Two ranging principle are mainly used: the pulsed ranging principle and, ranging by measuring the phase difference between the transmitted and received signal backscattered from the object surface[7]. The phase difference method uses the continuous wave lasers. Lidar technology is used as an active remote sensing in which light is used as its own source of energy. With the help of a self-generated laser, lidar technology can work in the dark and shadows too. Hence, the shadows, as well as night condition, does not affect the lidar performance; whereas passive remote sensing is extremely affected by these facts. The time difference between laser pulse being sent out and returned, the direction where the laser pulse is sent, and the absolute location of the sensor in respect to the earth plays the great role in the field of remote sensing. This information can eventually give the latitude, longitude, and elevation of the target [8]. Lidar is also not affected by the sunlight. However, lidar technology is affected by the weather condition because the laser cannot penetrate deep into the rain, fog and cloud and the laser beam cannot pass through the opaque obstacles. That fact makes lidar system challenging to detect target deep inside the forest and in other complex landscape.

1.5 Types and uses of lidar systems

There are two types of lidar technology based on the way the laser is generated: pulsed and continuous wave lasers. In remote sensing, round trip time of the emitted laser pulses is measured to determine the distance of the reflecting object.

Based on the types of the laser source, lidar again can be divided into various categories. For instance, some examples of such laser sources are CO_2(9.2 μm -11.2μm), Er:YAG(2 μm), Raman shifted Nd:YAG(1.54 μm), He-Ne(0.63 µm), GaAlAs (0.8 µm~0.904 µm), frequency doubled Nd:YAG (0.53 µm).

Broadly lidar can also be divided into polarimetric and non-polarimetric based on the ability to have polarimetric discrimination. Polarimetric lidar can provide polarimetric information from the target object whereas such type of work is not possible with non-polarimetric lidar.

Furthermore, experimental and commercial lidars are developed in different ways according to the purpose. Some of the widely used experimental lidars are scanning lidar imager of canopies by echo recovery (SLICER), shuttle laser altimeter (SLA), laser vegetation imaging sensor (LVIS), multibeam laser altimeter (MBLA), and geoscience laser altimeter system (GLAS). SLICER is the integration of laser altimetry and surface lidar techniques which can rapidly measure the vertical distribution of canopy surface area. The system is mainly designed with laser footprint of 415 m for the recovery of returns from the top of the canopy and the ground in the same waveform. Small, more sensitive footprint can also be designed to get the information about the individual crown of the tree[9]. SLA was designed for the space-based laser altimetry and lidar which covers a wide area of sea, cloud, forest, and land. SLA was aimed as a pathfinder for the operational space-based laser remote sensing devices. An airborne, scanning laser altimeter, LVIS, was developed by NASA's Goddard space flight(GSFC)[10]. It has a nominal footprint of 25m which typically operates at altitudes up to 10 km above the ground. NASA has a project named vegetation canopy lidar (VCL) mission to measure the structure and volume of

vegetation[11]. VCL is also planned to understand the climate change, land use, and some other environmental issues and estimate the global biomass too. MBLA was a part of VCL. GLAS is the first lidar instrument for the continuous global observation of earth. It was launched in January 2003 in ICESAT spacecraft to study the mass balance of polar mass sheets and their effect in the sea level, and to gain the valuable information to predict future for sea level change. The secondary objective of the mission is a study of the cloud, and aerosols in the atmosphere and measure the roughness, reflectivity, snow cover and sea cover characteristics.

Moreover, multiwavelength airborne polarimetric lidar (MAPL) has been developed in the University of Nebraska to support the airborne remote sensing program. MAPL laser sends out two laser pulses at the wavelength of 1064 nm and 532 nm at the same time. Silicon PIN detector is located at the top of the laser head which can monitor the relative output of the laser. Photomultiplier tube receives the backscattered light from the target and determines the state of polarization of light in both of the wavelengths[12]. Co-Polarized and cross-polarized light contain the valuable information about the target. Co-polarized light denotes the light which gets parallelly polarized with respect to the direction of emitted light. Whereas cross-polarized light denotes the light that gets polarized in an orthogonal direction with respect to the emitted light signal. Hence the polarization state in both parallel and perpendicular direction can be used to characterize the target. The various study claims that this polarization state is affected by biological and chemical properties of the target too. That is why it is very much useful in the field of vegetation, forestry, fishery and many other. Measurement of polarimetric information can provide the nitrogen fertilization, yield estimation and water stress condition of the plant.

Cloud structure study, soil classification, forest remote sensing, underwater fish study, target discrimination and other environmental monitoring can be the potential application field of MAPL. The polarimetric signature of any target can be extracted from the object and multiwavelength airborne polarimetric lidar, in fact, uses two channels at each wavelength and hence comparison can be made for cross and co polarization state of the target in between the two wavelengths.

Since 2004, these experimental approached lidar sensors were commercialized with full waveform system. Various companies all around the world also started manufacturing commercial lidars.

Based on the relative position of transmitter and receiver, lidars can be divided into monostatic or bistatic. In the monostatic configuration, transceiver and receiver are co-located. Monostatic configuration can be subdivided into two categories: coaxial and biaxial. The coaxial system has got a laser beam which is transmitted co-axially with the receiver's field of view. The biaxial system consists of transmitter and receiver adjacent to each other. Most of the modern lidar system are monostatic[13].

Based on the way of collecting the data, a pulsed lidar system can be classified as discrete return system, full waveform system, photon counting system and synthetic aperture lidar system.

Discrete return system

Discrete return lidar system records the individual(discrete) points for the peaks in the waveform curve. Each object encountered by the laser beam contributes individual scattering effect to sum up with multiple echoes. This system identifies the peaks and

records a point at each peak location in the waveform curve. These individual points are called returns. The system typically collects first and last pulses. Typically 1-4 or sometimes more returns from each laser pulse is recorded by this system[14].

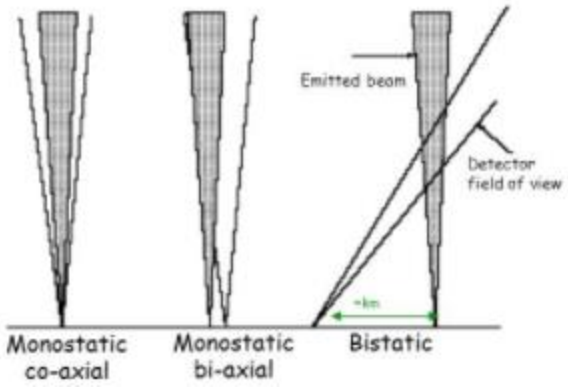

Figure 1.1 Lidar with different axial properties.

Full waveform system

Full waveform lidar is widely used later in comparison to discrete return system. Full waveform lidar system records all the history of the signal returned to the sensor over the series of equal length of time. Using the received signal, amplitude versus time plot can be constructed. This resultant waveform contains the information about light beam used for sensing purpose and the target. Advancement of full waveform interpretation increases the accuracy, reliability, and resolution of target and range detection.

Based on the footprint size, energy of pulse, property of polarization, PRF and operational platform, full waveform lidar system are of different types. Due to the big difference in these types, their accuracy and applications vary too. Information of recording interval inside the laser footprint causes the variation in detail. The rate of sampling of the backscattered waveform for a conventional full waveform system is at around 1

Gigasamples/s. However, digitization sample may vary from 1 to 10 ns, based on the lidar application. Full waveform lidar system is greatly implemented to find out either the target has horizontal or vertical distribution based on the operational platform. Processing of full waveform obtained from the sensor needs decomposition, segmentation, and classification. Decomposing the waveform into a sum of echoes can turn the data into a 3D point cloud[15]. However, instead of 3D cloud point, the captured signal might be taken into the 1D signal topology. Gaussian decomposition is one of the most popular methods of decomposing the full waveform of lidar. There are some other methods like averaged square difference function (ASDF) method and reversible jump Markov chain Carlo (RJMCMC) methods for decomposition. Segmentation of lidar data is performed before the classification of them. For the classification of data, various approaches are studied like width and amplitude parameters of the decomposed signal, together with some geometric features[16]. For recording the complete waveform, digitization terminal is also added to the system. Digitization results in the output into 8 bits.

Choosing the suitable footprint is also very important in full waveform lidar application. Full waveform lidar with large footprint can collect large forest canopy information including the multiple elements of the bigger forest. So, if the coverage is a major issue of interest, larger footprint full wave lidar is a better option. If collecting the information from a small portion of the forest element is the aim, then small footprint laser should be implemented. Small footprint can detect the top part of a tree or individual tree element. While forest is under the research, the top of the canopy, crown or underlying layer and ground surface, all are important. But based on the interest and area of the place, type of lidar can be varied. Lidar sensor is very much sensitive at the level of few photons

per unit interval. So even a tiny part of vegetation can alter the return waveform projecting the feature of the canopy. Even in the worst-case scenarios like a low intensity, overlapping echoes, and multiple echoes, full waveform lidar can detect the signal disregarding the number of peaks. If the emitted pulse is recorded, later fluctuation in the observed intensity with respect to the emitted pulse can be evaluated. The determination of the cross-section of the target from the backscattered signal is also possible which can help on removing the effect of various losses on received signal imposed by Lambertian reflectors[17].

Photon counting system

Photon counting lidar system is the advancement of the traditional lidar system which uses low energy resources with high altitude operation capability which ultimately offer a longer laser lifetime and a large area of coverage. Traditional lidar system emits a series of high-intensity pulses at low pulse rate but this latest advancement emits a multitude of low-intensity pulses at the high-frequency rate. Mostly this latest system is utilized in the green wavelength(532nm). This instrument offers an eye-safe working environment because of low laser energy despite operating at a visible wavelength. PRF of the system can be controlled in a better way because detection is based on single photon return. The principle outcoming of this system using green wavelength is that photon returns from the emitted pulse and photon resulted from ambient noise cannot be separated. To reduce the background noise, small field of view for the detector and narrow optical bandpass filter is recommended. Coincidence filter can be used to remove the rest of the background noises[18].

Synthetic aperture lidar

This newly emerging lidar technology eliminates the diffraction limit of the imaging system and there is no limitation of resolution by aperture size. For both air-borne and space-borne technology of lidar, this synthetic lidar is implemented in radio frequencies. Synthetic aperture lidar and SAR are similar in some angle. SAR utilizes the shorter optical wavelength and that allows more information acquisition within the short time period of data collection. Platform motion gives the advantages to coherently sample the multiple sections of the aperture. Final resolution SAR image is created using the coherent reconstruction of all the backscattered returns. Synthetic aperture lidar(SAL) operate at 1000 times smaller wavelength than SAR that makes the resolution of SAL to be tens of millimeters[19].

CHAPTER 2 LITERATURE REVIEW

2.1 Introduction

Researchers have worked to characterize the plant throughout the different times of the year and tried separating the various species based on those characteristics. Types and structure of different plant in a broader area are very important in the wildlife preservation and balance of the ecosystem. However, it is extremely complex to collect the field data from a bigger area with various plants mixed everywhere. Detection and classification of the plant need a remote sensing system that can differentiate minute changes in the composition of the plant. Remote sensing of vegetation went through the various stage of maturity.

2.2 Passive remote sensing

Some of the examples of passive remote sensing are areal imagery system, satellite photography and land survey. Terrestrial imaging spectroscopy was also one of the widely used technique. Reflected electromagnetic energy of sunlight from an object is dispersed into the spectrometer and get a continuous spectrum[20]. Each pixel from the object can form a complete spectrum. Hence object information can be extracted from the spectrum. High spectral resolution remote sensing becomes popular and use of various ranges of the spectrum. Then airborne imaging spectroscopy (AIS) was developed. The airborne visible/infrared imaging spectrometer (AVIRIS) and portable instant display and analysis spectrometer (PIDAS) were the two spectral systems which make a lot of difference in early remote sensing technologies. These studies were funded with NASA earth observation system (EOS)[21, 22].

Phenological variation of the plant throughout the season is useful in differentiating one specific species from other at specific times of the year[23]. Thomas Key *et al.* tried to differentiate four different types of tree species based on the imagery taken by light aircraft nine times from May to October 1997 using both true color and false color infrared film. Study of phenology was proven to be very important to find out the land cover of various plants and keep track of every plant in the forest. Even if the variation of characteristics may be caused by a various factor, photography was used on the project to get some seasonal variations. They have claimed that multispectral data obtained from this system got valuable and important information and they can provide the classification of different species of plants.

Early methods utilize an imaging technique to observe the phenological change of plant. The accuracy of imagery remote sensing depends on the type of imagery and other photographic characteristics like shape, timing, resolution, shadow, the texture of imagery and measurement scale. Major drawback of classical photography is, this depends on illumination of sun light and extremely hampered by shadows and other weather conditions like rain, snowfall, clouds etc. Aerial photography is not sufficient to gather the information from the lower layer of canopy and ground level. This system typically loss a lot of canopy information because of image resolution, atmospheric disturbance, motion and vibrational effect of aircraft. Later hyperspectral and high-resolution sensors were used to improve the surface feature information and separating small features of canopy. But passive remote sensing still had limitation on giving the information of canopy in vertical distribution. Airborne data acquisition pattern was implemented to reduce this limitation.

Burkholder *et al.*[24] in 2011, study on the separability of the seasonal trend of leaf reflectance in invasive ailanthus from four other native plants using passive remote sensing technique. Spectral factor measurement was done using ASD Field Spec Pro full-range (350nm to 2500 nm) spectroradiometer. White reference spectrum was obtained using white background and software was used to find out the ratio. Selection of spectral band as well as time of data collection changes the accuracy of classification. Asner *et al.* in 2008 found that the difference in leaf structure, water content and biochemical composition could give spectral signatures used to differentiate the various species from each other[25]. Use of high spatial resolution airborne visible and infrared imaging spectrometer (AVIRIS) provide the reflectance signatures of Hawaiian native trees from other invasive trees which were found to be linked with leaf pigments like chlorophyll and carotenoids, nutrients like nitrogen and phosphorus, and structures of leaf like specific leaf area and leaf area index. Hawaii[25] experiment provided a wide possibilities of differentiation of plant species based on spectral imaging and later Burkholder *et al.*[24] made a discovery in seasonal separability of various plant based on the reflectance parameter.

Somers *et al.* in 2012 studied the hyperspectral time series analysis of some native and invasive species in Hawaiian rainforests[26] using spaceborne imaging spectroscopy technology. Studied have been done for two native species and other two invasive species with the use of spaceborne imaging technology. Seasonal study was done by taking picture of species 22 times over four years of time and spectral separability was the major goal. This seasonal separability could be one of the major monitoring, mapping and detection technique of native and invasive species. Separability index (SI) was used to quantitatively

compare the various species and SI was found to be unique in Hawaiian trees than the invasive species in the near infrared region. But separability was not prominent throughout all the year for near infrared range and the spectral band is the better way to compare all species. They have concluded that differing life strategies and functional properties of various plant species directly showed a variation of spectra.

2.3 Lidar remote sensing

All these passive remote sensing imagery techniques were heavily dependent on atmospheric conditions and passive energy source like the sun. The best way to reduce the dependency and limitation is using the optical remote sensing with its own illumination source, i.e. active remote sensing. Lidar is one of the optical active remote sensing technique. Different platforms and systems of lidar can be implemented, for example, discrete return, full waveform, airborne, spaceborne, as well as ground based lidar. Choosing the right platform of lidar can give information on tree height, biomass, leaf area index, foliage height profile and so on. The classification of tree species can be done using the lidar. In 2008, Voss *et al.* studied about the seasonal effect on tree species classification in an urban environment using hyperspectral data, lidar, and an object-oriented approach[27]. They used two airborne imaging spectrometers for hyperspectral images and lidar to differentiate size, shape, the height of the tree to make easy separation of certain tree species. Seasonal data analysis was done for fall and summer season with 57% accuracy for summer dataset and 56% for fall dataset using hyperspectral classification. The use of lidar increased the classification accuracy by 19% for both summer and fall. This improvement is possibly caused by the removal of the shadow effect and addition of some more elevation data which separate high and low vegetation. Here on the same work,

lidar system showed its potential to be a better remote sensing. Before this study, the researcher already used lidar system to detect and analyze the individual leaf and tree crowns to establish the relation between crown structure and the plant species[28].Statistically, significance differences were detected in numerous species of trees using the small footprint, high sampling density lidar data.

There are some other researches on Lidar application to classify the vegetations based on the physical structures like the height of the tree, diameter and length of the crown, stem positions and shapes and structures etc. In 1997, Naesset *et al.* used airborne laser scanner data to estimate the forest tree canopy height[29]. He calculated the tree canopy height model (CHM) as the difference between the tree canopy hits and corresponding digital elevation mode l(DEM). Hence, Canopy height model represents the height of the tree as a raster dataset. Popescu *et al.* in 2002 apply a median filter to smooth the CHM for improved estimation of individual tree crown width[30]. In 2004, Clark *et al.* used the small footprint airborne laser scanner for the determination of sub-canopy elevation and height in the tropical rain forest landscape[31]. Local minima algorithm was developed to separate overlying vegetation return and lidar ground returns which were fully automated. Then various geostatistical techniques were used to interpolate the meso-scale digital terrain models (DTMs). DTM is one of the lidar products which is widely used in the research of tropical rain forest ecology. This is a discrete return lidar system. Sub-canopy elevation estimation accuracy was affected by the vegetation cover and steepness and complexity of forest structure. Again, In the year of 2005, small footprint airborne laser scanner data was used to create a canopy height distributions which used both first and last pulsed data [32]. Laser scanning was used to compute the height percentiles, mean and

maximum height values, canopy density at different height intervals, and coefficient of variation of height. In addition, small footprint lidar was used to calculate the leaf area index of the plant along with the estimation of the height of tree and crown dimensions[33]. In the study, tree heights were estimated quite accurately. Estimating the leaf area index (LAI) was generally very costly and involved intense field work but remote sensing techniques have made the work significantly easier. Lidar was sensitive enough to estimate the individual tree leaf area index. The accuracy was found to be better than those obtained from the ground-based measurement system.

Solberg *et al.* later used the airborne laser scanner data for the single tree segmentation in a structurally heterogeneous spruce forest. Data thinning, surface modelling, identification of local maxima, and development of segments around each of these maxima are the four major steps used by them. In this study, optimization was done in canopy surface model to have better control over the shape of crown segments. In this single lidar return system, only the first return echoes were used. Tree height, crown base height and crown diameter were estimated with the optimization and smoothing model. Data filters were applied to the data to get better accuracy and removal of unwanted local maxima[34].

New object oriented small footprint lidar algorithm was described by considering the clusters of trees as an object of interest[35]. In this object-oriented approach, a group of adjacent pixels was used as an object rather than individual pixel as shown in Figure 2.1. Considering the adjacent pixels in the object of interest helped on the extraction of information because covering more pixel increased the chances of not losing any valuable features from being extracted. However, the process is computationally expensive, and the

pixel of the image needs to be smaller than object interest. When the result object from the object-oriented approaches are directly compared with the individual tree algorithm, tree clustering approach performed better in density evaluation and volume, height, crown width and biomass estimation too.

The local maxima method used above have a lot of depending variable conditions. Small footprint airborne laser altimetry is used with the improvement in the local maxima method by a smoothing filter. The study area of black hills forest consists of rocky

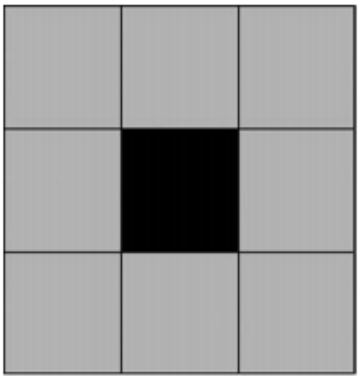

Figure 2.1 Idea of using a group of pixels where core pixel (black) and edge pixel (grey) are considered as a part of tree cluster.

mountain area with managed tree species and elevation ranges from 1500 m to 1800 m above the sea level. Algorithms named virtual deforestation algorithm used a despiking algorithm to smooth the bare earth digital elevation model (DEM). By using the Canopy height model and with some modification to improve the classification, tree height, individual crown width, and individual tree stem were detected. A lot of smoothing over CHM model was done and significant improvement was obtained over the stem count of the individual tree[36].

All the above mentioned lidar system are discrete lidar return systems. Discrete return system characterizes the 3-dimensional forest canopy structure. The beginners of airborne laser scanner can provide only one backscattered echo per emitted pulse. But when there are multiple targets with in the footprint, multiple pulse laser scanning is needed. Many multi echo systems collect first and last pulses. Later, instead of recording only one or few more backscattered echo, full waveform lidar technologies are developed which can measure all the echoes. Full wave lidar can record the detailed geometric and radiometric information of canopy return [37]. A lot of full waveform lidar technologies are also used to enhance the performance and accuracy of data extraction. Digitization terminals are designed by the manufacturers so that the terminals of the lidar can record all backscattered energy as a function of time. Very high storage capacity is also needed for the purpose.

Reitberger *et al.* in 2007 studied delineating a single tree from the jungle and also detecting the stem position based on the small footprint full waveform lidar. [38].They use the CHM and watershed algorithm to determine the stem point, ground point, and crown point too. This was another work using the lidar. However, full waveform method does have certain limitation in success rate in case of the heterogeneous forest where trees are to close from one another. Still, digitization of full waveform pulse of the reflected laser provides more information on the object. Reitberger *et al.* in 2008 describe a way to classify deciduous and coniferous trees using the small footprint full waveform lidar system[39]. The pulse width and intensity of reflected laser beam were extracted from the waveform decomposition which also gives the 3-dimensional coordinates of the object. Unsupervised classification of pulse width and 3-dimentional coordinates of reflections detected deciduous and coniferous trees. Clustering of data into coniferous and deciduous

class gave overall 85% accuracy in a leaf-on the situation and 96% in the leaf-off situation. Although the waveform decomposition is computationally complex, it contains the vital information of the object from which light gets reflected. This method has its advantage over the discrete return lidar.

Mallet *et al.* in 2009 published a literature survey on full waveform topographic lidar [40].Full waveform lidar is used to detect and identify many forest and woodland parameters in the past. Canopy height, vertical and spatial distribution of forest was estimated from the differences between the height of last and first echoes, in all kinds of forests like temperate, boreal and tropical[41]. Scanning lidar imager of canopies by echo recovery (SLICER) lidar was used to obtain the airborne laser altimeter waveform and utilized to determine the vertical distribution of deciduous forest. It also defined the occlusion rate of plantation[42]. Researchers tried to identify canopy cover, canopy volume profile, above-ground biomass, basal area, mean stem diameter, crown and stem volume and many other parameters like the density of trees using the waveform method of lidar.

Cao *et al.* in 2014 used both the discrete lidar and full waveform lidar system separately and collectively to see how they are related to each other[37]. Estimation of total biomass and its components in the forest for the understanding of carbon cycle was done with stepwise regression model in all three cases and all of them gave a satisfactory result. Metrics analysis for the properties of tree related to height like mean height, upper height percentiles, the height of median energy (HOME) and Vertical distribution ratio (VDR) were done with very good prediction and accuracy by both discrete and full waveform methods. Full waveforms were more sensitive to the foliage biomass and trunk biomass and this method have certain improvement over discrete method in the characterization of

the vertical structure of the forest. But in most of the cases coupling of both discrete and full waveform matrices gave better accuracy and increased performance.

Full waveform lidar is considered as a good way to obtain a better backscattered profile on various popular platforms. Full waveform method is better than discrete system because it can obtain the continuous information directly from the vegetation with better accuracy and efficiency. Presently, the major lidar technique has spaceborne, airborne and terrestrial laser scanning. Study about the plant vegetation is implemented using different platforms and their efficiency and accuracy depend on the various field of study. To obtain the information for vertical positions and to the ground level, terrestrial remote sensing is a great plan. Spaceborne and airborne systems are also very much useful for the horizontal profile as well as for various angle of information.

2.4 Study of plant physiology

Remote sensing can get information related to the physiological and seasonal variation of the plant. Chlorophyll variation throughout the season can be studied. Another fact that can cause variation is occlusion of the plant. Xylem and phloem of plant tissue conduct water, synthesized food, salts, minerals and provide the mechanical support. This vascular occlusion of the plant has a certain seasonal behavior and remote sensing can detect the seasonal change on it. Koniger *et al.* in 2000 studied the physiological changes in the shade leaves of sugar maple leaf. They found that average photosynthesis rates remained high during the summer and started to decrease in early September[43]. This decrement is accompanied by the decrease in leaf pigment, protein and nitrogen concentration.

Asner *et al.* pointed out the possibilities that measured signal from the passive optical remote sensing of vegetation canopies were contributed by both the canopy structure and biochemical properties of canopy structures[44]. They discovered that leaf reflectance varied more widely in certain plants like Yucca Plants. For the thicker plant leaf with more water, they found different transmittance than another leaf with thin structure. Also, this variation is not the same in different regions of the optical wavelength. This finding is very important and could be implemented in lidar too. It is expected that the spatial configuration of backscattered returns in the point cloud coupled with the intensity values of airborne lidar can be used to classify the tree species. Later, Kotz *et al.* used radiative transfer modeling to estimate the forest fire possibilities relating to the canopy structure, leaf area index and foliage water condition[45].

A lot of passive remote sensing was done for the study of plant physiology and biochemistry which is also explained in the passive remote sensing section of this chapter above. Later due to the limitations of passive remote sensing, active remote sensing is started to complement the passive one for the study of plant physiology.

Morsdorf *et al.* in 2009 assess the physiological information of plants of the forest using multispectral lidar waveform by radiative transfer model[46]. Simulation of the multi spectral waveform was done for single scots of pine trees of various ages and various stages of growing season, which include the fact of changing chlorophyll concentration over the time. That means they performed a seasonal prediction on the plant leaf. This full waveform multispectral canopy lidar (MSCL) proved itself useful in identifying the tiny change in leaf optical properties with ages and different physiological conditions of the plant. Koetz *et al.* in 2007 fused an imaging spectrometer with lidar data over combined

radiative transfer models to characterize the forest canopy[47].Basically, lidar was used for the assessing of horizontal and vertical canopy structure of forest whereas imaging spectroscopy was used in assessing biophysical and chemical properties of the plant.

2.5 Polarimetric measurements

2.5.1 Polarimetric imagery remote sensing

Modern remote sensing has the greatest challenge to classify, identify all kinds of targets either in the military battlefield or in the geo-environmental stress change monitoring purpose of civilian people [5]. Data quality is the major factor for the precision and accuracy of classification and identification. Various active and passive polarimetric sensors are implemented for this purpose. Polarimetric measurement is already widely accepted in the research field. Passive imaging polarimetry uses the imaging polarimeter as a polarimetric sensor. Optical radiation of any target contains various information about the distribution of object which can be measured by spectral imagers which range from multispectral to hyperspectral. Polarization information may reveal the shape, roughness and surface feature of the object. Also, the contrast changes of an object with respect to its surrounding help to find the surface features within the absorption band [20]. The intensity of the image gives the ability for polarization to enhance the contrast. But still, this passive polarimetric imagery system solely depend on the reflection of sun light and hence weather, time, and location of sensor greatly affect the accuracy of data obtained. Hence active polarimetric remote sensing is greatly implemented as polarimetric lidar.

2.5.2 Polarimetric lidar remote sensing

Polarization lidar remote sensing has a great start with the atmospheric research[48]. Polarization lidar was a key technique for the weather investigation and

finding out the type of cloud on the sky [48, 49]. Polarimetric lidar is also used in forestry and vegetation as well as earth surface study. In the active lidar system, linearly polarized visible or near infrared laser is illuminated on the target and backscattered light is sensed by the receiver system. Parallel and perpendicular component of backscattered light is separately measured with the help of linear polarizer at the receiver. Resolving two components of polarization is the major aspect in polarization lidar system. Characterization of the different polarization state of backscattered light is done by various optical instruments like polarimeter. The polarization state of laser source, as well as polarization state of backscattered light together, can provide the polarization property of the target. For a single wavelength of the laser source, the receiver can detect backscattered light of linearly polarized laser source parallel and perpendicular to the polarization of the emitted light. Parallel backscattered light with respect to the emitted light is called co-polarized light and perpendicularly backscattered light with respect to the emitted light is called cross-polarized light. The detector system may be of a single channel or double channel. They can also be categorized as a single detector type and dual detector type. Single detector type can detect either co-polarized or cross-polarized light at one time, but it has sequential switching property. Dual detector type has the ability to detect simultaneous dual polarization. In recent cases, a co-polarized and cross-polarized component of backscattered light is measured by dichroic beam splitter followed by a photomultiplier tube combined with a narrow-band interference filter centered at either 532 nm or 1064nm according to the laser source[50]. In most cases, linear or circular depolarization ratios are used to classify the target particle like a cloud, ice and so on. But completely spherical depolarization sometimes turns out to be zero depolarization. In most

cases both the depolarization ratios deviate from zero; and depending on the particle size and property, this value is unique. Polarization sensitivity is also useful in lidar measurement in applications such as vegetation, fish and insect detection.

So far it is well established that reflections of actively generated plane electromagnetic wave done by scattering surface carry very important information about the scattering surface and this is the foundation of recent active polarimetric lidar remote sensing. Polarization state changes after the reflection of the wave from the surface; and relationship can be established between the polarization phenomenon and property of the reflecting surface. There are many examples of active remote sensing systems used for earth surface, underwater study, and vegetation study. When active electromagnetic wave like light pulse is passed through seawater, different polarimetric transformation will occur in the light pulses according to the target under water which can be analyzed and interpreted [51]. Hybrid microwave radar and lidar system were also proposed in the detection of a shallow underwater target to have a better performance including the plus points of both of the systems[52]. First multispectral radiometric and polarization measurements of the earth's surface using a polarized laser light source were claimed in 1993 with the airborne laser polarization sensor(ALPS)[53].

Tan *et al.* in 2005 used the multiwavelength polarimetric lidar to obtain the polarimetric reflectance and depolarization ratio from the several tree species[12]. They found out that tress species can be separated from one to another using the depolarization ratio and it could be an efficient way to identify the tree species. Tan *et al.* in 2009 used multiwavelength polarimetric lidar for foliage obscured man made object detection[54]. The work demonstrated that polarimetric reflectance from the manmade surface can be

differentiated from the foliage polarimetric reflectance and the key is to choose the right wavelength of the laser. The fact that reflectance differs from one object to another opened a lot of possibilities of using the polarimetric lidar in differentiating various objects. This opens the door of research to try differentiating one plant from the other and same plant at different condition and time.

2.6 Research objective and motivation

No research has been done to see the seasonal change of the depolarization ratio of any species of plant. As Tan *et al.* already tried differentiating several species of plants [12] using the depolarization ratio and also demonstrated the ability of polarimetric lidar to differentiate plant foliage from man-made object [54] and Morsdorf *et al.* modeled the seasonal behavior considering the different chlorophyll concentration[46], it is possible to see the future of lidar in real time seasonal change detection. Also, the variation of pigments, nitrogen, and protein along with the rate of photosynthesis of plant after the beginning of September[43] can be studied using the lidar. So, a major goal of this study is to see how plant leaf shows the changes in depolarization ratio as season changes and how polarized lidar behaves with it. Maple tree leaf was chosen as it is widely available, easy to collect, and it also changes the color from fall season towards winter. Moreover, characterizing the dryness of the vegetation leaf is another goal of the thesis. Dryness of leaf can provide us the chance of fire catching by forest. Dryness of leaf in the agricultural field can provide the necessity of irrigation in the crop lands. Hence the motivation of the thesis is characterizing the plant leaf based on the seasonal changes as well as based on the dryness using the novel technique of polarimetric lidar system.

CHAPTER 3 EXPERIMENTAL SETUP AND DATA COLLECTION

3.1 Experimental setup

In this study, the near-infrared polarimetric lidar system was selected to measure the depolarization ratio from polarimetric reflectance. An Nd:YAG laser (MIL-III-1064 50 mW, Model No.16090761) was used as a source of illumination in the experiment. Near-infrared light at a wavelength of 1064-nm was used which send the linear vertically polarized laser beam. This is a continuous wave laser with the transverse mode of TEM00 which uses the DPSS (diode-pumped solid state) laser technology. TEM00 laser has a gaussian intensity profile. Laser controller and power supply were used to control and monitor the power to the laser. The instrument, optical chopper MC2000B, utilizes the advanced features to create the pulsed light from a continuous beam. The chopper blade MC1F10HP whose frequency ranges from 20 Hz to 1 KHz was used. The chopper was used to control the frequency of the detected signal to the photodetector. When the frequency of chopper was increased, the frequency of the signal detected by the photodetector was also increased. The linear polarizer and the TE-series photodiode were used to detect the amount of reflected laser light in different polarization states. The linear polarizer has set on a rotary optical mount which allows 360 degree rotation for optical angular positioning[55]. This mount could be rotated to zero degrees to obtain the co-polarized reflectance and to 90 degrees to obtain cross-polarized reflectance form the target. Rotating the mount to zero degree means letting the reflected signal which is parallel to the transmitted wave to pass through, and rotating the mount to 90 degree means

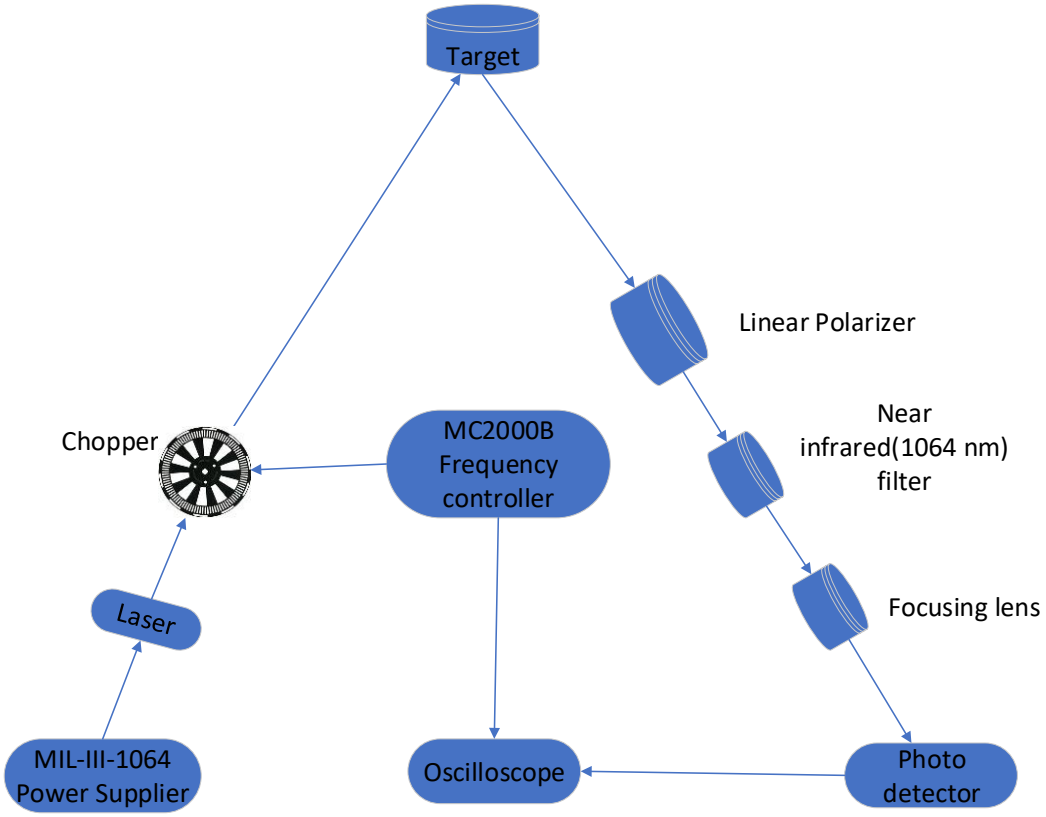

Figure 3.1 Schematic experimental setup for measuring the depolarization ratio.

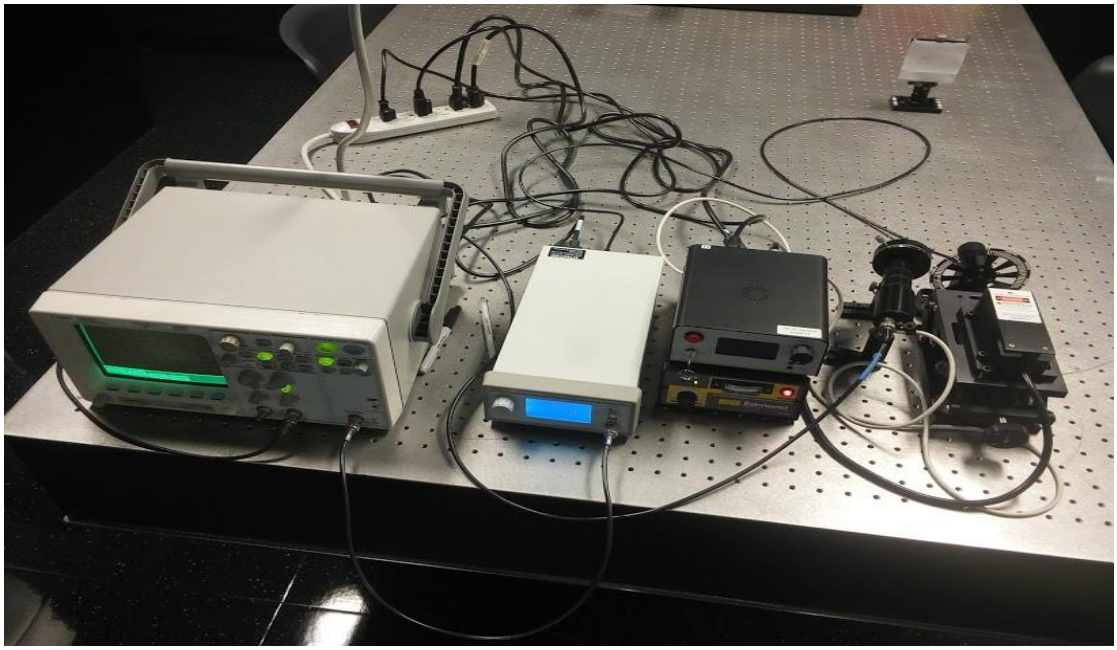

Figure 3.2 Experimental setup for polarimetric lidar measurement system.

letting the reflected signal which is perpendicular to the transmitted wave to pass through. Receiver module has a detector type of 3 mm InGaAs photodiode operated with a thermoelectric cooler for stabilization/cooling with a build-in FET transimpedance amplifier. The output voltage is proportional to the input signal current, i.e.$V_{out} = I_{signal} * R_f$ where R_f stands for feedback resister of the amplifier. Agilent 54622A oscilloscope with two channels and a bandwidth of 100 MHz was used to collect the electrical signal generated by the photodetector. The oscilloscope had 200 MS/s sampling rates and 2 Mbytes of megazoom deep memory per channel. Photo detector and oscilloscope were connected as shown in Figure 3.1.

Figure 3.2 shows the experimental setup with a laser, chopper, target, polarizers, and photo-detector which were kept on the table. Photo detector was mounted and cannot move, so the angle of reception is fixed. When polarizer was rotated to a different angle, it will pass only specific linearly polarized component of light towards the photo detector to receive. For example, when the polarizer was set to zero degrees, only the co-polarized signal will pass through it. The gain of photo detector was set to the maximum level. When the photo detector receives the optical signal and converts it into an electrical signal, it is sent to the oscilloscope to have a real time view of the signal generated by the photo detector. In addition, the oscilloscope was set to average 512 waveforms. Since a single measurement waveform is noisy, the averaging technique was implemented because the noise was uncorrelated. Averaging was done automatically by the oscilloscope and the averaged signal was displayed. Hence final averaged measurement of cross polarization and co-polarization were recorded, and the depolarization ratio was calculated.

3.2 System calibration

In every experimental setup, calibration is important to insure the consistency of measurement. In this experiment to ensure that the setup is not changed, and the polarizer and receiver were at the same locations, calibration was done every time before the measurement. Laser power and chopper frequency were made consistent for every measurement. In this experiment white paper was used as a calibration standard to measure the reference depolarization ratio value. At the beginning of every experiment, the depolarization ratio of white paper was measured. In every further experiment, before taking a measurement on any object, the white paper test was also done, and the depolarization ratio value was observed to be consistent. Average depolarization ratio for the paper at the beginning was obtained to be 0.941071 and the standard deviation was 0.012421 for all the data.

If μ is the average and σ is the standard deviation,

$$\mu + \sigma = 0.941071 + 0.012421 = 0.953492 \quad (3.1)$$

$$\mu - \sigma = 0.941071 - 0.012421 = 0.92865 \quad (3.2)$$

In all the future measurement, when paper reference was within the 1-sigma value of this reference, it was considered as an acceptable reference and continued the experiment on that setup. The histogram plot for the depolarization ratios measured on paper reference at the beginning is shown in Figure 3.3. The distribution of depolarization ratio values is close to gaussian. Also, the measurement of laser power at different polarization angle under the paper target was done to verify that the system was working correctly. The summary of that measurement is shown below in Table 3.1:

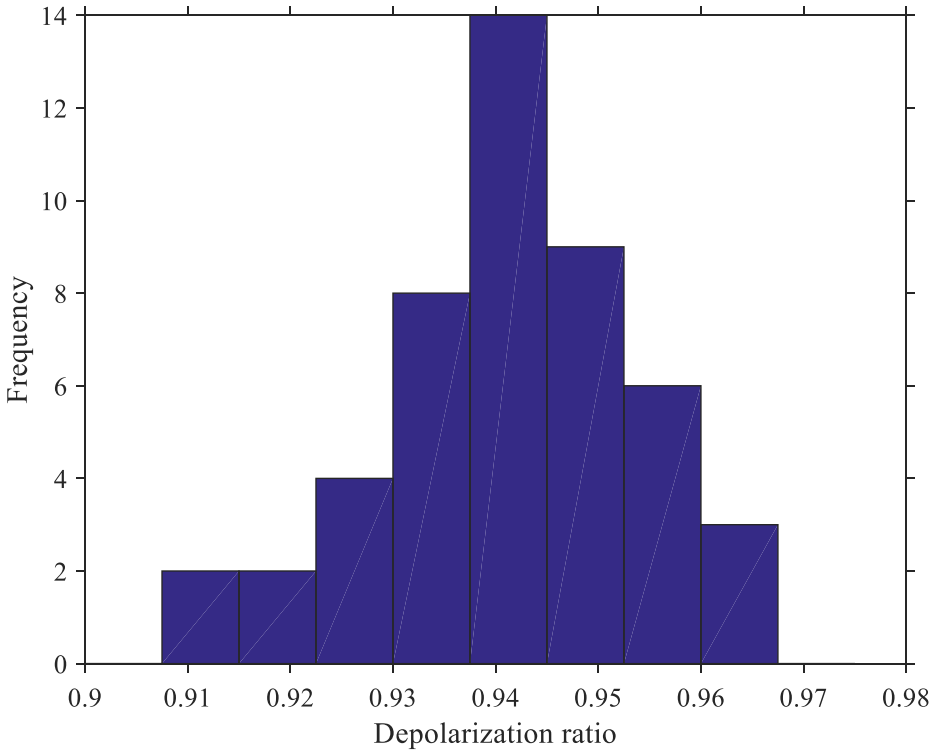

Figure 3.3 Histogram plot for the depolarization ratio of initial standard paper reference used for calibration.

Table 3.1 Laser power at different polarization angle difference for paper target.

angle Difference	0 degree	28 degrees	45 degrees	68 degrees	90 degrees
1	31.39	31.45	31.05	30.41	29.53
2	31.6	31.41	30.98	30.02	29.59
3	32.09	31.66	31.05	30.12	29.57
4	31.7	31.56	31.09	30.08	29.65
average	31.695	31.52	31.0425	30.1575	29.585

The measurement of laser power was done with polarizer angle set at 0 degrees. This is the beginning point of measurement and considered as a 0-degree angle differenced point. Then angle was changed towards 90 degrees by 28-degree, 45-degree, 68-degree and finally by 90-degree. Zero-degree point is considered as co-polarization and 90 degree point as cross-polarization. When the angle difference in polarization was decreased from 90 to 0, laser power values keep rising from 29.585 to 31.695. This shows that the experimental setup is working correctly. Optical reflectance of the laser is higher at co-polarization which was expected to be. Depolarization ratio is always less than 1.

3.3 Procedure

The measurement of depolarization ratio was done in the dark room to reduce any other ambient noise. To take the measurement, fresh leaves were collected from the tree and kept in a zip lock bag. Zip lock bag kept the leaves from any kinds of damages on its surface and prevented the leaf from losing water. Efforts were made to keep the leaf fresh for measurement. But before making a measurement on a leaf, the white paper was mounted on the post and the laser was shined on the paper and the reflected polarized light was measured for both cross-polarized and co-polarized condition. Peak-to-peak voltage output for both cross-polarization and co-polarization was measured from the oscilloscope. After that, the depolarization ratio was calculated and see if the system was well calibrated or not. After making sure that system is well calibrated, the leaf was mounted on the post using 3M transparent tape and the reflected polarized light was measured and displayed on the oscilloscope. Finally, the depolarization ratio for the leaf was calculated and recorded. When the depolarization ratio was measured for one point on the leaf, laser power was turned off and the position of the leaf was changed. The process was done very carefully

so that the experimental setup was not moved. After that, when the laser beam was shined, it could measure the depolarization ratio of the same leaf at a different point on the surface. In this way, the depolarization ratio was measured for around 10 to 12 points of the leaf. The process was repeated for another leaf and depolarization ratio of each point on all the leaves surfaces were recorded on an excel sheet. Table 5.2 shows the number of leaves and number of measurements done each time. The depolarization values shown in table 5.1 is an average of all the measurements done on the specific time denoted on the table.

3.4 Data collection

Procedure for the measurement of depolarization ratio was already explained in the procedure section of this chapter. The maple leaf is easily available around Brookings, SD. And it has flat leaves, so it is suitable for the measurement. Furthermore, maple leaf shows a seasonal change in the color. The color of maple leaf changes from green to yellow and red. Hence Maple leaf was chosen for the seasonal study and experiments were conducted periodically throughout fall 2017. The same maple tree on the west side of South Dakota State University was chosen. Leaves were collected from the same side of the tree throughout the experiment. Measurements were done two to three days in a week and three different times within a day.

CHAPTER 4 THEORY

4.1 Scattering theory of lidar

Every surface of material either reflect the light or absorb it. Reflectance is of two types: Lambertian (diffuse) and Fresnel (specular). Two different types of surfaces are shown in Figure 4.1. When light strikes on the surface, reflected light intensity and the direction of reflection will be different according to the surface property. Perfectly smooth specular surface returns a single reflection at a line of sight direction. So that receiver will not receive any reflected signal unless it is kept in the line of sight. But most of the natural surfaces produce a lambertian reflection with signal scattered in all the directions. Glass, water, smooth-wet surfaces give specular reflectance but most of the other surfaces are rough in the sense of optical reflection causing the lambertian reflection. The backscattered signal is affected by the chemical composition, wavelength, polarization, and incidence angle of light. Object size, orientation and spatial distribution of targets, surface roughness and water content of plants are some of the important factors for the backscattered mechanism in the plant.

In the system of lidar, collimated lidar beam is sent through the transmitting medium, then interact with the targets of interest, and a fraction of the laser energy scattered back is collected by the lidar receiver. During the interaction of light with the target, polarization property and strength of laser beam get modified according to the target. Hence reflected light bears a lot of information about the target. The process of retrieving the information depends on the setup and system of lidar.

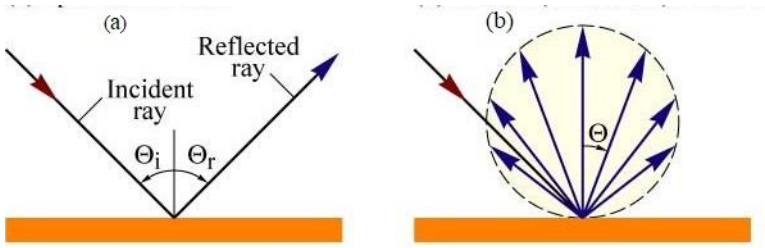

Figure 4.1 Two types of surface reflection of light namely (a)Specular or Fresnel(left) and (b)Diffuse or Lambertian(right).

4.2 Optical scattering model for a leaf

Light might be absorbed or scattered when it interacts with the leaf. Light conversion into heat, fluorescence, and other forms may happen. The pigments composition, distribution, and concentration, as well as distribution of water, affects the absorption of light in the infrared region. But absorption is very efficient in ultraviolet and visible regions[56]. Internal scattering of incident light happens inside the leaf which is controlled by the arrangement of tissues and cells of the leaf. Figure 4.2 shows the typical cross-section of a leaf. Refractive index of the layer of wax and surface roughness characteristics controls the reflectance of light. Typical thickness of leaf is about 1/10 to 1 mm. Reflection of light occurs mostly in specular direction and not depolarized much in surface wax [57]. However, this layer of wax in terms of thickness is varied a lot from plant to plant. The morphology of surface wax is dependent on the chemical composition of wax and it is determined either genetically or by the various parts of the plant[58]. The wavelength of light is also the important matter to see the polarization effect through the wax layer. In the case of optical frequency, the surface features are small enough compared with the incident wavelength, then the surface wax is optically smooth but undulating. The

polarization of light will be based on the Fresnel equation.

There is an assumption on leaf surface that roughness changing with water content on it. When the leaf water content decreases and thickness of leaf decreases, leaf cells dehydrate and collapses which increases the roughness of the wax layer[59]. Increased roughness decreases the specular reflection from the surface and certainly changes the factor of polarized light. Hence the ratio of the polarized and nonpolarized component may contain the moisture status information of any leaf.

Scatter of EM wave is a complex phenomenon inside the leaf surface because of the presence of complex cytoplasmic contents, refractive index variations among each layer, variable geographical organization of tissues and their irregular shapes. The chloroplast contains grana which are suspended in the cytoplasm, are of a 0.5-micrometer length and 0.05 micrometer in diameter. This size is in the range of wavelength of light.

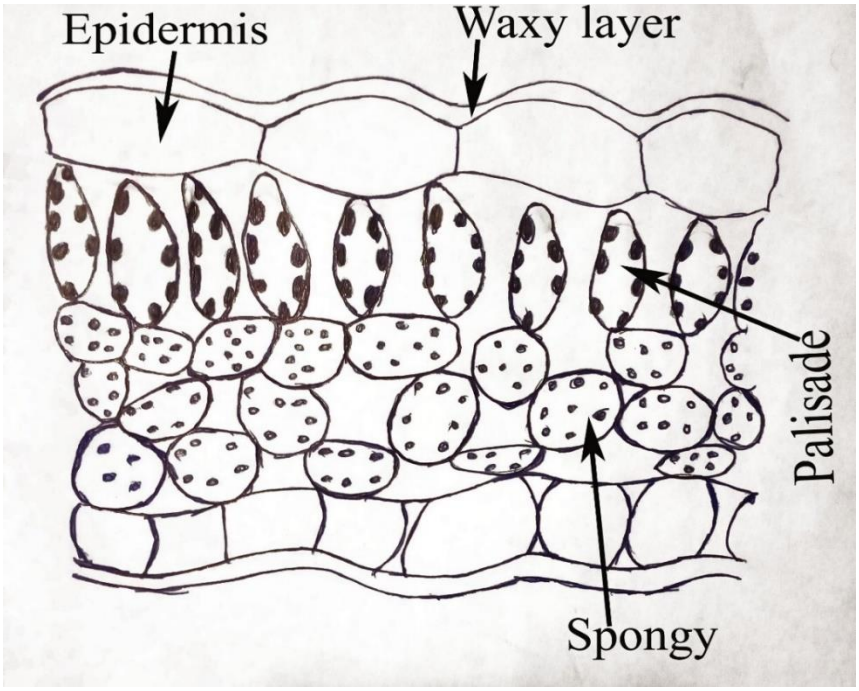

Figure 4.2 Typical leaf cross section.

Hence scattering of light mostly happens in this region. There are other structures like ribosomes, nuclei, starch grains etc. which are also of the dimension of light wavelength. Because of these structures, scattering is a complex procedure.

4.3 Polarization theory of light

The polarization of light can be presented in various ways and various mathematical representations. States of polarization also can be realized as polarized, partially polarized and non-polarized light. Polarization can also be divided into linear, circular and elliptical polarization.

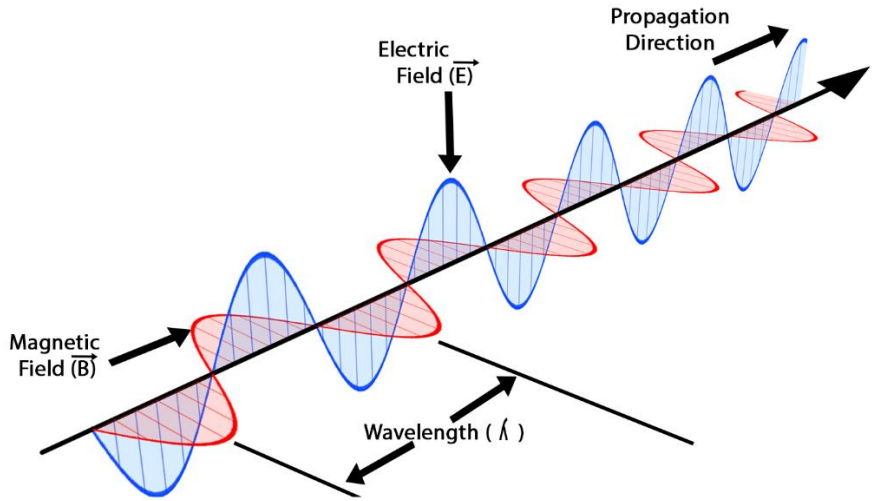

Figure 4.3 Orientation and propagation of the electromagnetic wave[60].

Light is the combination of mutually oscillating spatiotemporal transverse electric field, E(r,t) and transverse magnetic field H(r,t) which makes it an electromagnetic wave as shown in Figure 4.3. The wave can either be TE or TM based on the orientation of the plane of incidence. Perpendicular electric field to the plane of incidence is generated by TE wave whereas TM wave gives electric field parallel to it. Two plane polarized wave E(r,t)

and H(r,t) comprises of the electromagnetic wave and are sufficient to transmit the information about the target to the sensor. The speed of EM wave is the speed of light(c=3*10^8) in a vacuum. EM can be transmitted via air, vacuum, or any medium. Information is encoded in the form of intensity, frequency or polarization, which are used to acquire the information about the remote object.

Laser generally generates polarized light. That means waves all having the same frequency and zero or same phase difference are emitted by the coherent source of light. Polarized light can be represented by an electric field, **E**. For all the regions of space with zero charge or current, the direction of electric field is the key to determine the polarization condition of the electromagnetic wave. That means the orientation of the electric field determines whether light is elliptically or linearly or circularly or randomly polarized. As represented in Figure 4.3, electric field, magnetic field, and direction of propagation of wave are all perpendicular to each other. Both **E** field and **M** field can oscillate on any planes and direction. When **E** field oscillates in a plane then it is called linearly polarized light.

Let us consider the case when **E** field is oscillating in the plane between x and y-direction then, it can be decomposed into horizontal and vertical components. Horizontal and vertical components can be expressed in equations:

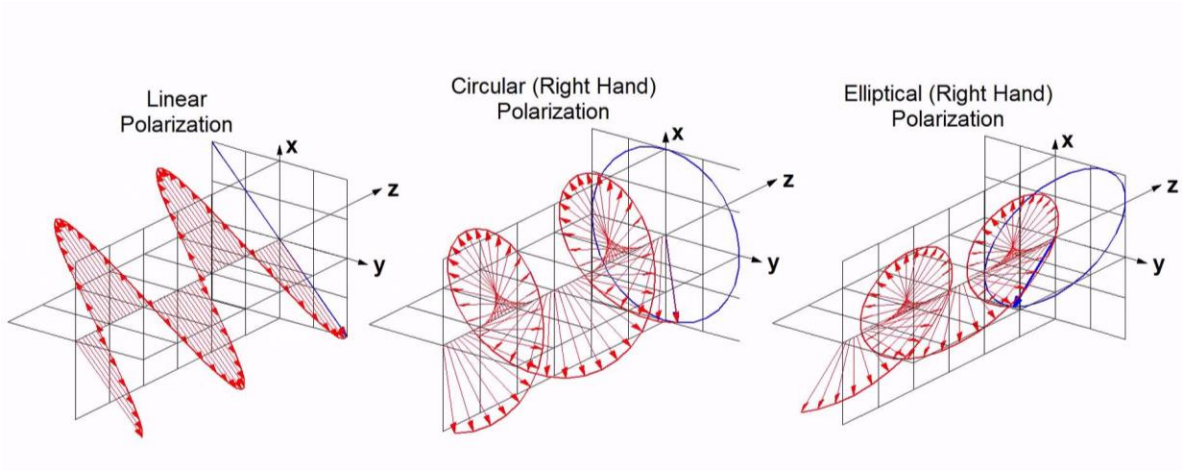

Figure 4.4 3-Dimensional view of different kinds of polarization[61].

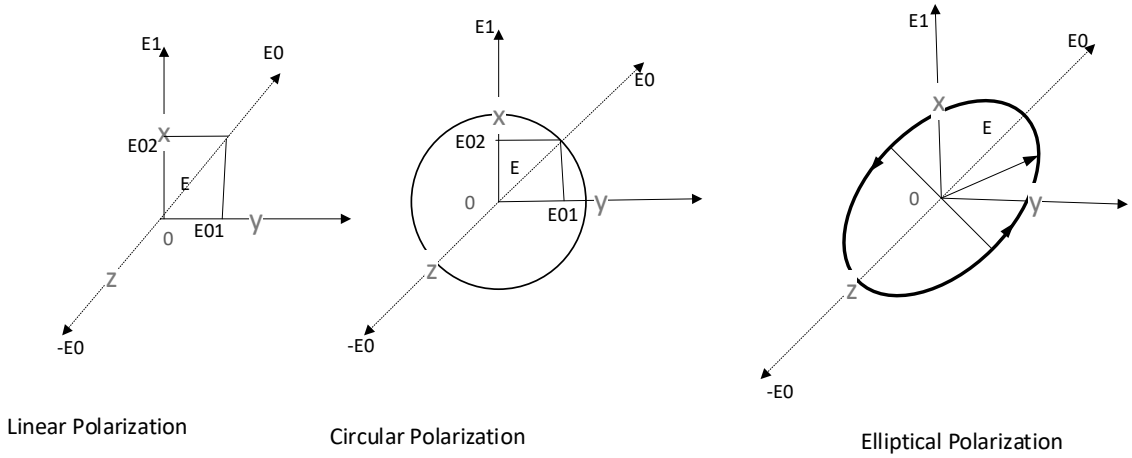

Figure 4.5 Geometrical representation of three types of polarization[62].

$$\boldsymbol{E}_x = \boldsymbol{e}_x E_{ox} \cos(\omega t - kz), \tag{4.1}$$

$$\boldsymbol{E}_y = \boldsymbol{e}_y E_{oy} \cos(\omega t - kz + \delta), \tag{4.2}$$

$\boldsymbol{e}_x$ and $\boldsymbol{e}_y$are unit vectors, E_{ox} and E_{oy} are the magnitude of field X and Y direction respectively, ω is the angular frequency, δ is the phase difference between the horizontal

and vertical component of the electric field and k is the wave vector in the direction of wave propagation which is z axis. Vectorially, such waves can be represented as

$$\boldsymbol{E}(z,t) = E_x(z,t) + E_y(z,t). \tag{4.3}$$

If $\delta = 0$ or integer multiple of π then two components, horizontal and vertical components are in the same phase and resultant electric field is linearly polarized. In that case, the resultant magnitude of the electric field will be

$$E = \sqrt{E_{ox}^2 + E_{oy}^2}. \tag{4.4}$$

And the resultant angle of the electric field, E with the x-axis is

$$\theta = \arctan\left(\frac{E_{oy}}{E_{ox}}\right). \tag{4.5}$$

When δ is not equal to zero and not equal to an integer multiple of π , the electric field will no longer be linear. It will be either elliptical or circular or random. In general, the tip of the **E** field traces the elliptical path and hence general equation for elliptical polarization will be:

$$\left(\frac{E_x}{E_{ox}}\right)^2 + \left(\frac{E_y}{E_{oy}}\right)^2 - 2\left(\frac{E_x}{E_{ox}}\right)\left(\frac{E_y}{E_{oy}}\right) cos\delta = \sin^2\delta. \tag{4.6}$$

The relative axis of an ellipse with the x-axis is known as azimuth angle denoted as α and expressed as:

$$\tan 2\alpha = \frac{2E_{ox}E_{oy}cos\delta}{E_{ox}^2 - E_{oy}^2}. \tag{4.7}$$

Phase difference δ determine the shape of an ellipse. When $\delta = \pm\frac{\pi}{2}, \pm\frac{3\pi}{2}, \ldots.$, then the equation becomes

$$\left(\frac{E_x}{E_{ox}}\right)^2 + \left(\frac{E_y}{E_{oy}}\right)^2 = 1, \tag{4.8}$$

which resembles the circle. So, in this condition polarization becomes circular.

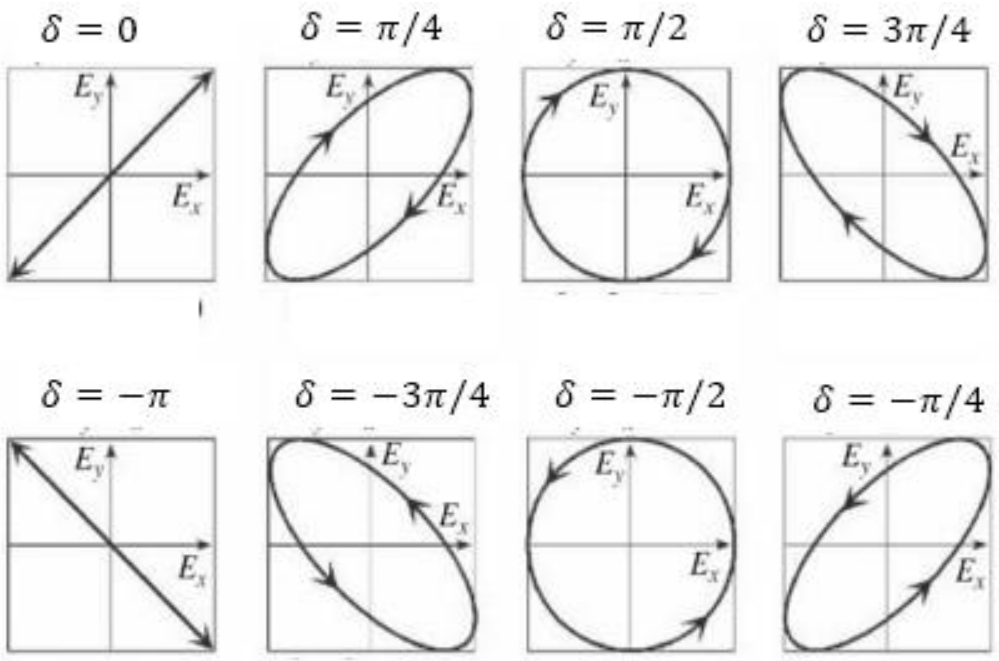

Figure 4.6 Phase difference and their types of polarization[63].

There are different ways of representing the polarization states. Some of them are jones representation, trigonometric representation, complex plane representation etc. Each of them has its advantagefor certain specific nature of polarization states. There is also the Stokes vector representation which introduces some measurable parameters.

4.4 Stokes parameters and depolarization ratio

Stokes parameters relate the intensity of light with one another. Polarization information is presented in various mathematical terms with the combination of intensities. Matrix representation of Stokes parameters with four- element parameter is shown below:

$$S = \begin{bmatrix} I \\ Q \\ U \\ V \end{bmatrix}. \tag{4.9}$$

Where I= total irradiance, Q= horizontal linear polarization, U= +45 degrees linear polarization, V= right circular polarization component of light, which are called stokes parameters. They can be related to a horizontal and vertical component of the electric field(E).

$$\begin{aligned} I &= E_{ox}^2 + E_{oy}^2, \\ Q &= E_{ox}^2 - E_{oy}^2, \\ U &= 2E_{ox}E_{oy}cos\delta, \\ V &= 2E_{ox}E_{oy}sin\delta. \end{aligned} \tag{4.10}$$

These parameters are related to the intensities with the relations:

$$\begin{aligned} I &= I_x + I_y, \\ Q &= I_x - I_y, \\ U &= I_{+45^\circ} - I_{-45^\circ}, \\ V &= I_R - I_L. \end{aligned} \tag{4.11}$$

Where $I_x, I_y, I_{+45^\circ}, I_{-45^\circ}, I_R, I_L$ are light intensities in their respective direction denoted by subscript.

One way to quantify the stokes parameters is by measuring I_1, I_2, I_3, I_4, the outputs from horizontal, vertical, $+45^\circ$ polarizer, and quarter wave followed by $+45^\circ$ linear polarizer. Then the Stokes parameters can be obtained by

$$I = I_1 + I_2,$$
$$Q = I_1 - I_2,$$
$$U = 2I_3 - I_1 - I_2, \quad (4.12)$$
$$V = I_1 + I_2 - 2I_4.$$

The depolarization ratio can be defined as the ratio of vertical to horizontal polarizer outputs. In other words, depolarization ratio is the ratio of reflectance cross-polarization to the reflectance co-polarization value.

Depolarization ratio,

$$D = \frac{I_2}{I_1}. \quad (4.13)$$

The degree of polarization is used to explain the percentage of total light intensity which gets polarized.

The degree of polarization, $P = \frac{\sqrt{Q^2+U^2+V^2}}{I}$. (4.14)

For totally polarized light $I = \sqrt{Q^2 + U^2 + V^2}$ which makes polarization P=1 and for perfectly unpolarized light P=0, and in other case it will be in between 1 and 0. Azimuth angle, α can be expressed as $tan2\alpha = \frac{U}{V}$, which indicates the deviation of eclipse axes from the horizontal X-axis.

CHAPTER 5 STUDY OF SEASONAL CHANGE IN DEPOLARIZATION RATIO OF MAPLE TREE LEAF

5.1 Introduction

The objective of this research is to characterize the seasonal change in a maple leaf. The changes occurring inside the maple plant leaf with time was analyzed by measuring the depolarization ratio using the lidar system. The maple leaf was plucked from the maple tree found inside the South Dakota State University. Depolarization ratio was measured for the maple leaf collected from mid-August to mid-December. For the consistency of the measurement, the same maple tree was chosen all the time; and visibly healthy and grown leaf was selected. Leaves were always plucked from the same side of the plant too.

5.2 Measurement of depolarization ratio for the maple leaf

At first, reference depolarization ratio was measured for the white paper as described in section 3.2. The measurement was repeated for 48 times. Then every time before starting the measurement on a maple leaf, depolarization ratio was measured for the standard white paper. All the white papers were new, unfolded and believed to have the same smoothness. Every time the white paper test was repeated for around 5 times. Before the first measurement on a maple leaf, the average value of depolarization ratio on white paper was calculated to be 0.938804 that is within the 1-sigma value of the paper reference. In this work, changes in maple leaves were analyzed within the day and between the days. Two Maple leaves were collected three times a day; morning, afternoon, and evening; and depolarization ratio was measured for each sample to study the changes within the day and the same procedure was repeated throughout fall 2017.

Figure 5.1 Sample maple leaves used for measurement throughout fall 2017.

Table 5.1 clearly demonstrates how the depolarization ratio value changes throughout the measurement period. Each leaf was measured 10 to 12 times and the number of leaves as well as the number of measurements on each leaf is summarized in Table 5.2. Table shows that there were sufficient number of measurements on each leaf. Each data point in the table is the average of a total number of measurements done over 1 to 3 leaves. Each leaf contains around 10 to 12 measurements all over the surface of the leaf.

Measurement spots were selected in a way so that measurement of depolarization ratios was done all over the surface of the leaf in a uniform fashion. After completing the measurement at one point, the leaf was unmounted and moved to the next point on the surface. In this way, 10 to 12 measurements were done over the leaf surface and finally averaged in Table 5.1.

Table 5.1 Table of all the depolarization measurement on maple tree leaves throughout the season.

date	average depolarization ratio each day			average depolarization ratio so far this date in			Average depolarization ratio all day
	morning	afternoon	evening	morning	afternoon	evening	
19-Aug	0.96672	0.97053	0.96747	0.96672	0.97053	0.96747	0.96881
24-Aug	0.96149	0.96641	0.96584	0.96324	0.96847	0.96638	0.96458
26-Aug			0.96703			0.96664	0.96703
29-Aug		0.96969	0.96611		0.96888	0.96649	0.9679
31-Aug	0.96864	0.96599	0.97029	0.9658	0.96816	0.96733	0.96831
2-Sep	0.96664			0.9646			0.96664
5-Sep	0.96802	0.97140	0.96555	0.96626	0.96881	0.96701	0.96833
7-Sep	0.96785	0.96808	0.96353	0.96655	0.96869	0.96647	0.96649
12-Sep	0.96830	0.96419	0.9655	0.96682	0.96804	0.96634	0.966
14-Sep	0.96546	0.96431	0.96353	0.96664	0.96739	0.96601	0.96442

19-Sep	0.96641	0.9633	0.96884	0.96661	0.96696	0.96631	0.96619
21-Sep	0.96522	0.96246	0.96469	0.96646	0.96653	0.96616	0.96413
26-Sep	0.96312	0.96226	0.96235	0.96614	0.96616	0.96583	0.96508
28-Sep		0.96052	0.96255		0.96571	0.96556	0.96153
30-Sep	0.96497			0.96604			0.96497
2-Oct	0.95851			0.96573			0.95851
3-Oct	0.95988	0.96441	0.96149	0.96549	0.96561	0.96526	0.96233
5-Oct	0.95781	0.96160	0.95966	0.96467	0.96533	0.96487	0.95942
8-Oct	0.96207			0.96458			0.96207
10-Oct	0.95857		0.96092	0.96419		0.96462	0.95975
12-Oct	0.95719	0.96416	0.96075	0.96377	0.96522	0.96438	0.96119
14-Oct		0.95927			0.96504		0.95927
17-Oct	0.95742	0.96424	0.95680	0.96341	0.965	0.96395	0.95949
19-Oct		0.95600			0.96451		0.95600
21-Oct	0.95905		0.95985	0.96317		0.96373	0.95945
24-Oct	0.96246	0.95815	0.95843	0.96315	0.96419	0.96346	0.95912
26-Oct	0.95972	0.95566	0.9582	0.96298	0.96377	0.96320	0.95786
29-Oct	0.95527			0.96279			0.95527
31-Oct		0.93282		0.96256			0.93282
2-Nov		0.94096		0.96159			0.94096

Table 5.2 shows the total number of measurement performed and the number of leaves involved. On the date of August 19, 4 leaves were used all together, and there were 48

measurements in total. We can see that one leaf has 12 data points. But one data point, in fact, was the average of 512 measurements and was averaged automatically by the oscilloscope as described in the system calibration section.

Table 5.2 Number of maple leaves and data points measured through the season.

Date	number of data points				number of leaves			
	morning	afternoon	evening	total	morning	afternoon	evening	total
19-Aug	12	24	12	48	1	2	1	4
24-Aug	24	24	24	72	2	2	2	6
26-Aug			24	24	0	0	2	2
29-Aug		24	24	48	0	2	2	4
31-Aug	24	24	24	72	2	2	2	6
2-Sep	24			24	2	0	0	2
5-Sep	24	24	24	72	2	2	2	6
7-Sep	24	24	24	72	2	2	2	6
12-Sep	24	24	24	72	2	2	2	6
14-Sep	24	36	24	84	2	3	2	7
19-Sep	24	24	24	72	2	2	2	6
21-Sep	24	24	24	72	2	2	2	6
26-Sep	24	24	24	72	2	2	2	6
28-Sep		24	24	48	0	2	2	4
30-Sep	24			24	2	0	0	2
2-Oct	12			12	1	0	0	1

3-Oct	12	24	24	60	1	2	2	5
5-Oct	36	24	24	84	3	2	2	7
8-Oct	12			12	1	0	0	1
10-Oct	24		24	48	2	0	2	4
12-Oct	24	36	24	84	2	3	2	7
14-Oct		12		12	0	1	0	1
17-Oct	24	24	24	72	2	2	2	6
19-Oct		24		24	0	2	0	2
21-Oct	24		24	48	2	0	2	4
24-Oct	12	24	24	60	1	2	2	5
26-Oct	24	24	24	72	2	2	2	6
29-Oct	12			12	1	0	0	1
31-Oct		20		20	0	2	0	2
2-Nov		24		24	0	2	0	2
	Total number of data points			1520	Total number of leaves			127

Some important trends can be extracted from the experimental data by analyzing the change in the depolarization ratio with respect to time. Time series plot for daily measurement is obtained so that we can see where this measurement is approaching. Last two rows on the table on October 31 and November 2 were measured after snow and it does not follow the trend line. So, these measurements were not included in any of the charts and time series plot below. In those last two measurements, leaves were dry and

already started to shrink. Those leaves were wrinkled and dry because of snowfall and hence are not considered in further analysis.

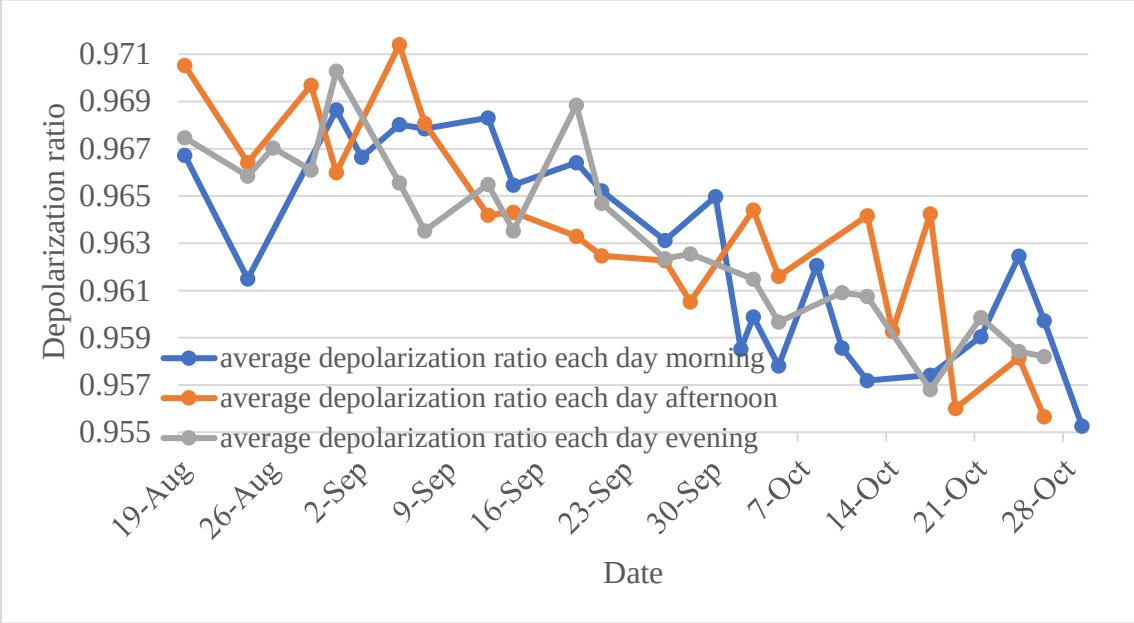

Figure 5.2 Time series plot for depolarization ratio measured at different times of different days.

Figure 5.2 is the time series plot of the depolarization ratio according to their date and time of measurement. Morning, afternoon and evening measurements are plotted separately to see the difference between them. A running average plot was obtained by adding all previous measurement until that time and then doing average on data, see Figure 5.3. Running average make the plot smoother. Figure 5.4 was plotted by averaging daily measurement, and the different times of the day were not considered here.

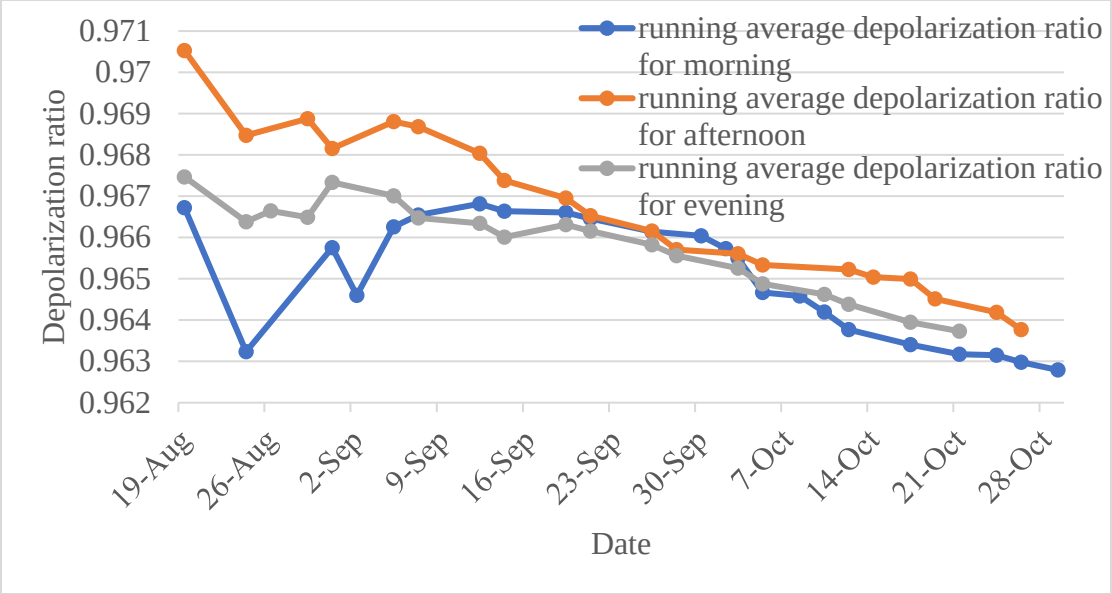

Figure 5.3 Running average plot for depolarization ratio.

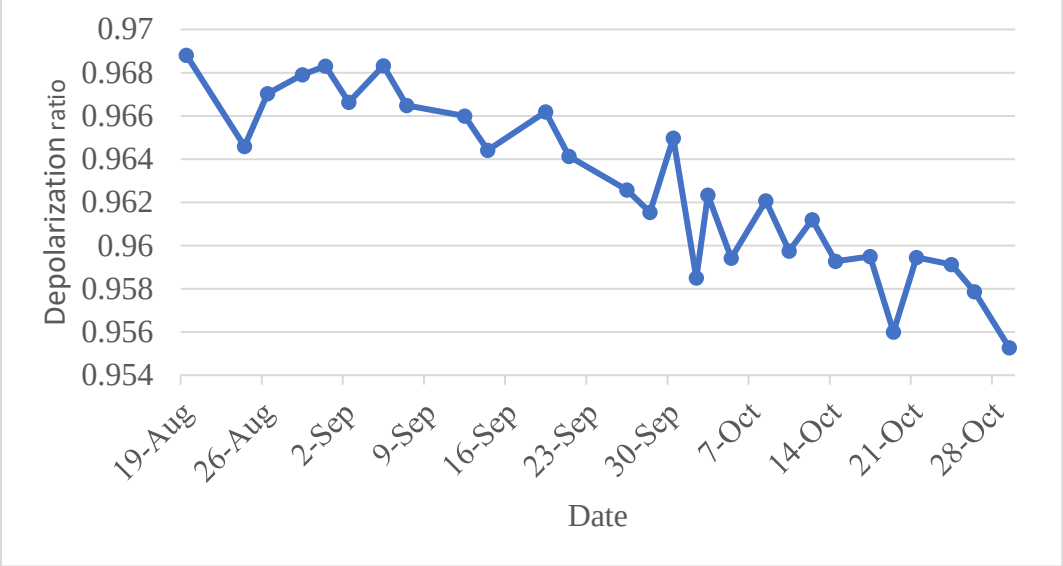

Figure 5.4 Time series plot for daily depolarization ratio.

All the time series plots show a clear downward trend of depolarization ratio values as season changes. The slope is not very steep, but the trend is consistent. Depolarization ratio value was at around 0.968 in the beginning, but it has decreased to around 0.955 at

the end before the first snow fall. After the snow fall, the depolarization ratio has a dramatic decrease to around 0.94.

The histogram was plotted for all the data points throughout the measurement period. Each data points belongs to the averaged depolarization ratio value of each measurement day. That means the measurement was done at three different times of the day, and the average was calculated from all measurement of that day. The histogram gives close to gaussian curve as shown in Figure 5.5. In Figure 5.6 histogram fitting was also done using the MATLAB (red line) and a vertical (blue line) was drawn indicating the peak of the histogram.

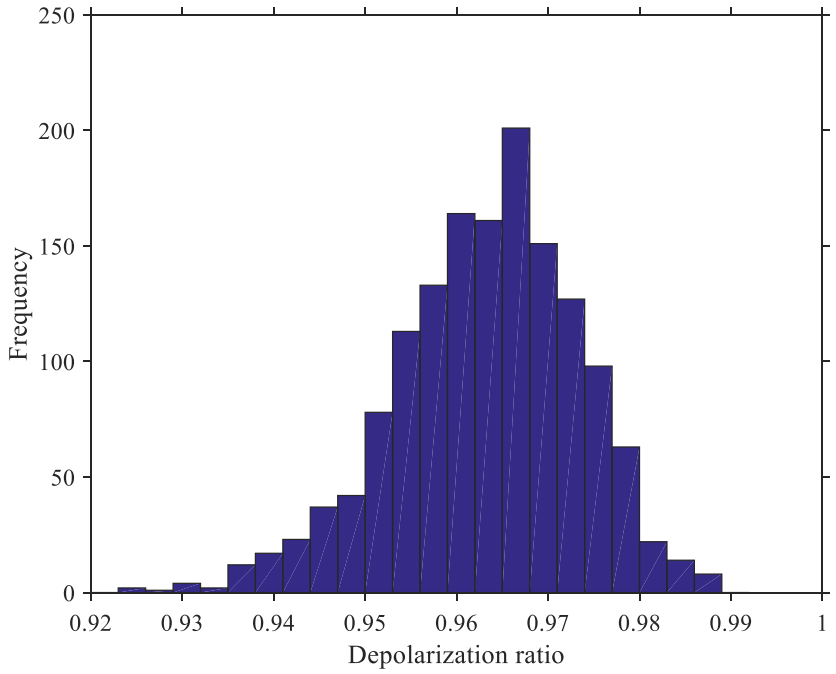

Figure 5.5 Histogram for all the measurement of depolarization ratio on maple leaves.

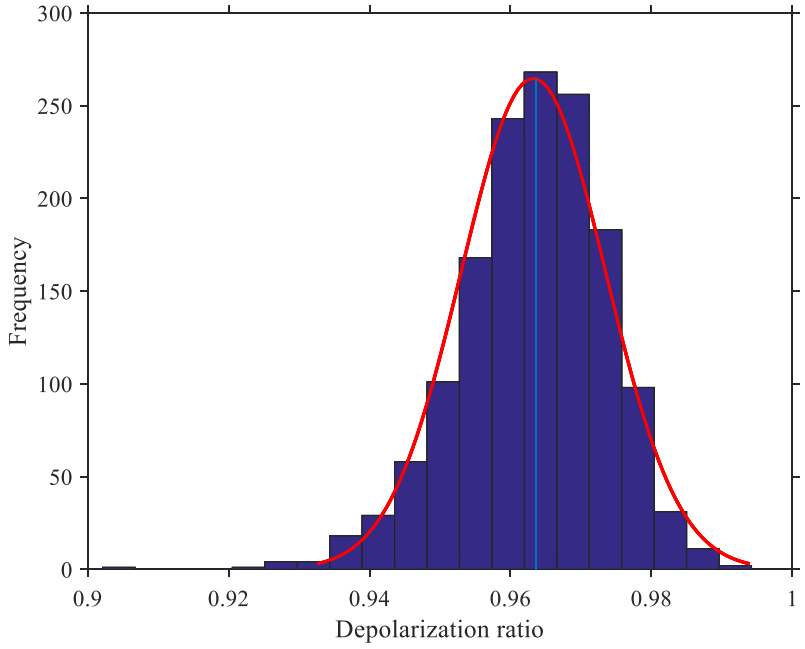

Figure 5.6 Histogram fitting for all depolarization ratio of maple leaves.

Histogram fitting is done using the *histfit* function in MATLAB which does the normal distribution fit. To quantify the normal distribution, mean and standard deviation of the data are needed. Normal distribution probability density function is:

$$f(x) = \frac{1}{\sigma\sqrt{2\pi}} e^{-\left(\frac{(x-\mu)^2}{2*\sigma^2}\right)} \tag{5.1}$$

Where, σ is the standard deviation, μ is the mean and x is the depolarization ratio. Default number of the bin is equal to the square root of a total number of elements in the data. Vertical line drawn from the maximum point of the fitted curve shows the co-ordinate of the maximum point as (0.9636, 264.5476). X-value is the depolarization ratio value. The average value of the depolarization ratio directly calculated from the excel sheet was 0.962502. By comparing these average values with the maximum point of depolarization ratio values on the histogram curve, we can say that they are close enough to conclude that

maximum depolarization ratio value of histogram gives an average of the total data.

5.3 Week by week change in depolarization ratio value

Day by day change in depolarization ratio was analyzed in the table and plot above, but we can also compare the result week by week. Histogram, which was close to gaussian, was plotted for measurement obtained each week. Histogram fitting was performed using MATLAB. Maximum values of histogram fittings for ten weeks are summarized in Table 5.3. Each value in the table is an average depolarization ratio measured in that week.

Table 5.3 Summary of depolarization value of maple leaf for each week.

week	morning	afternoon	evening
1	0.9636	0.9687	0.9669
2	0.9679	0.9681	0.9684
3	0.9682	0.97	0.9648
4	0.9671	0.9645	0.9648
5	0.9661	0.9632	0.9671
6	0.9643	0.9616	0.9628
7	0.9587	0.9633	0.961
8	0.959	0.9632	0.9612
9	0.9585	0.9604	0.9586
10	0.9596	0.9573	0.9586

The obvious downward trend of depolarization ratio can be again seen from the time series plot. This weekly analysis filters out more daily noise and agrees with the downward trend obtained from the day by day measurement graph.

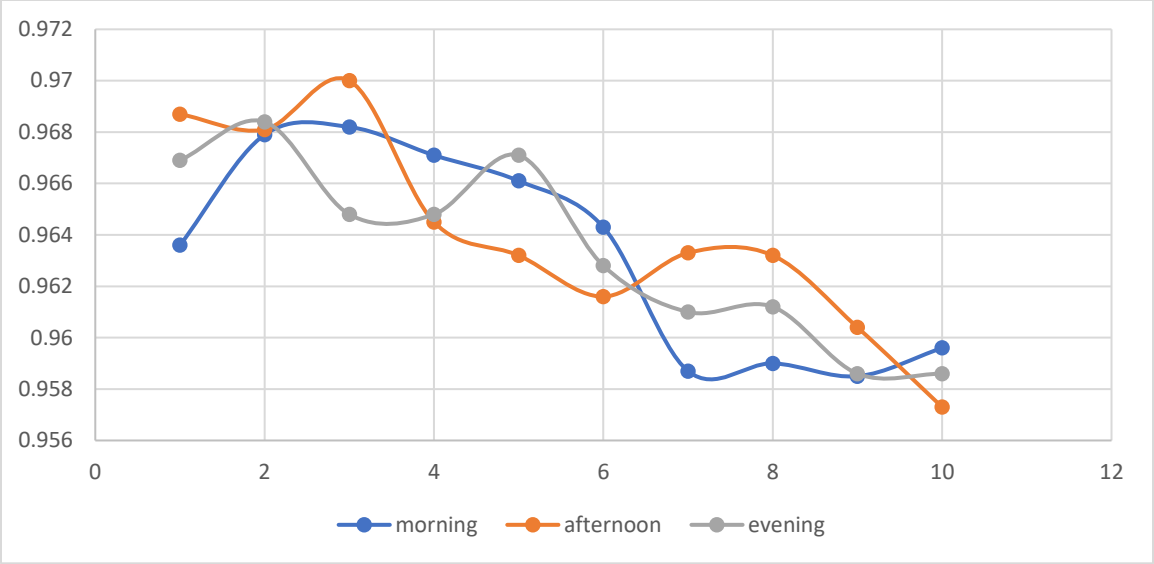

Figure 5.7 Time series plot of depolarization ratio considering each week as one data point.

5.4 Trendline of morning, afternoon and evening depolarization ratio values

The time series plot obtained above from the day by day measurement was considered for obtaining the linear trend line. The trendline is important to characterize the curve. Linear fitted equations and other parameters are shown in Table 5.4.

Table 5.4 Parameters obtained from linear fitting of time series curve of depolarization ratio.

	Fitted equation	R^2	Adjusted R^2	R_{mse}
Morning	y = -0.0001x + 7.2696	0.5981	0.579	0.0027
Afternoon	y = -0.0002x + 8.5124	0.5904	0.5699	0.0059
Evening	y = -0.0002x + 7.4344	0.7669	0.7547	0.0018

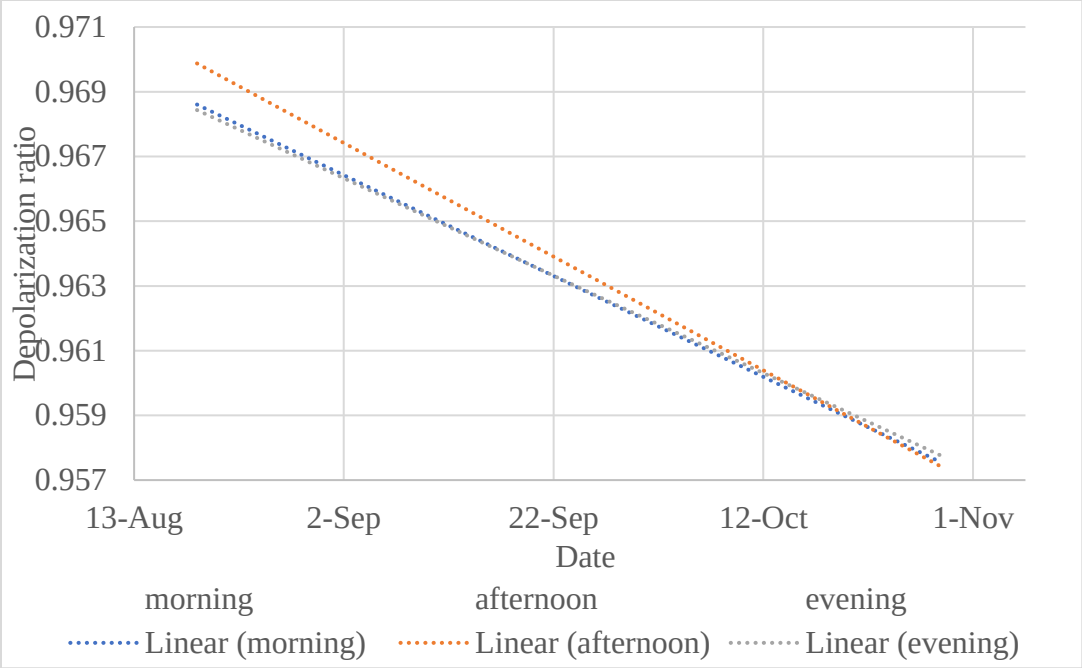

Figure 5.8 Linear trendline for time series depolarization ratio plot of maple leaves.

To check another possible curve fitting, second order polynomial was also plotted. The parameters obtained from the second order polynomial is shown in Table 5.5. Original curves

Table 5.5 Parameters obtained from second order polynomial fitting of time series curve of depolarization ratio.

	Fitted equation	R^2	Adjusted R^2	R_{mse}
Morning	$y = -1E\text{-}06x^2 + 0.1242x - 2666$	0.6179	0.5797	0.0027
Afternoon	$y = -3E\text{-}07x^2 + 0.022x - 468.82$	0.7097	0.6791	0.0051
Evening	$y = -1E\text{-}06x^2 + 0.0902x - 1934.6$	0.7793	0.7548	0.0018

are hidden and only the fitted curves are shown in Figure 5.8 and Figure 5.9. Morning and

evening fits are very close with each other whereas afternoon fit looks somewhat separated from rest two. Linear fit also shows that with an increase in time, all three curves try to converse in the same place. Polynomial curve fitting looks better than linear because of the relatively high value of R square and R^2 value. This indicates that it is not a linear decrease in the depolarization ratio with time.

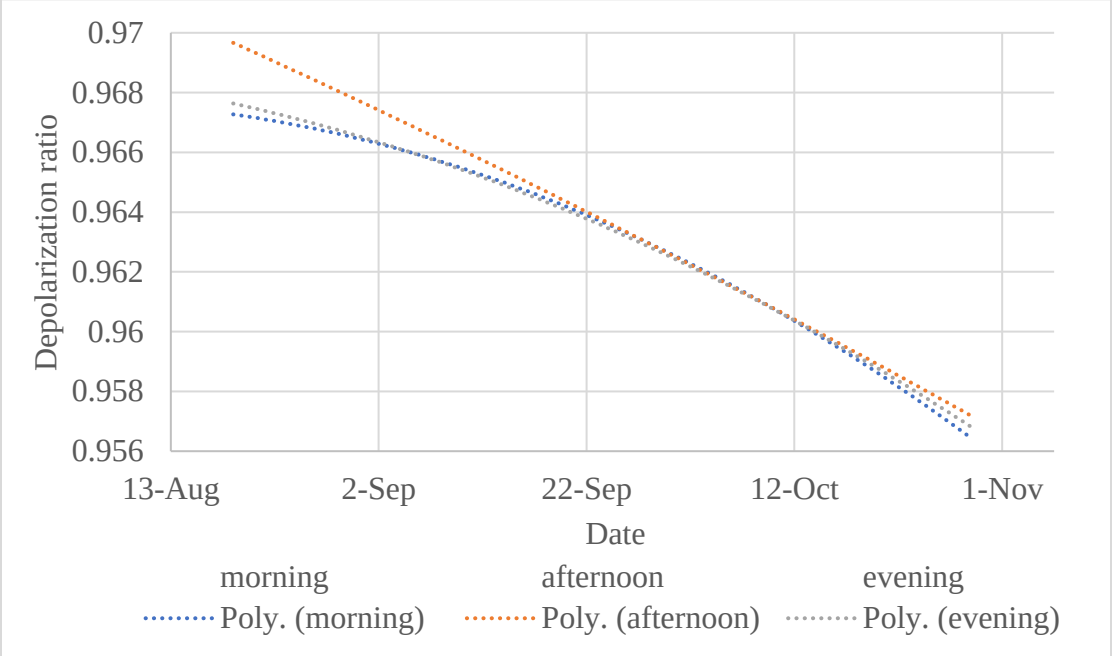

Figure 5.9 Polynomial fitting of time series depolarization ratio of maple leaves.

5.5 Histogram fitting for depolarization ratio at three different times of the day

Histogram fitting for morning depolarization ratio, afternoon depolarization ratio, and evening depolarization ratio were done separately as shown in Figure 5.10 to Figure 5.18. This histogram was plotted from all the measurement of depolarization ratio throughout the season. Histogram fitting for the depolarization measurements of the morning, afternoon and evening separately also give a close to a gaussian distribution. Gaussian distribution signifies that enough number of measurements was done to make

any statistical analysis. Vertical lines are drawn from the maximum points of each fitted curve so that we can clearly see the difference in their shift. The depolarization ratios corresponding to the maximum frequency are found out from MATLAB. The Value obtained from MATLAB in morning, afternoon and evening are 0.9631, 0.9641 and 0.9635 respectively.

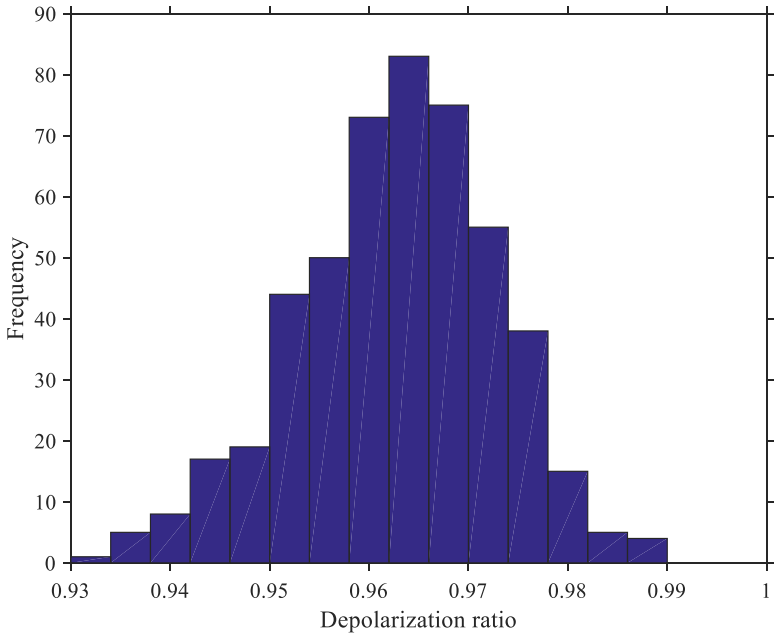

Figure 5.10 Histogram for morning data.

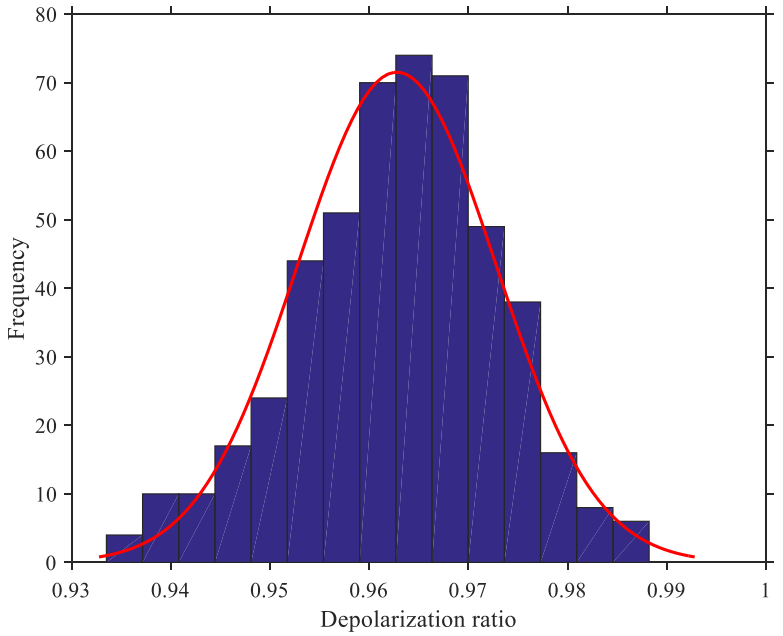

Figure 5.11 Histogram fit for morning data.

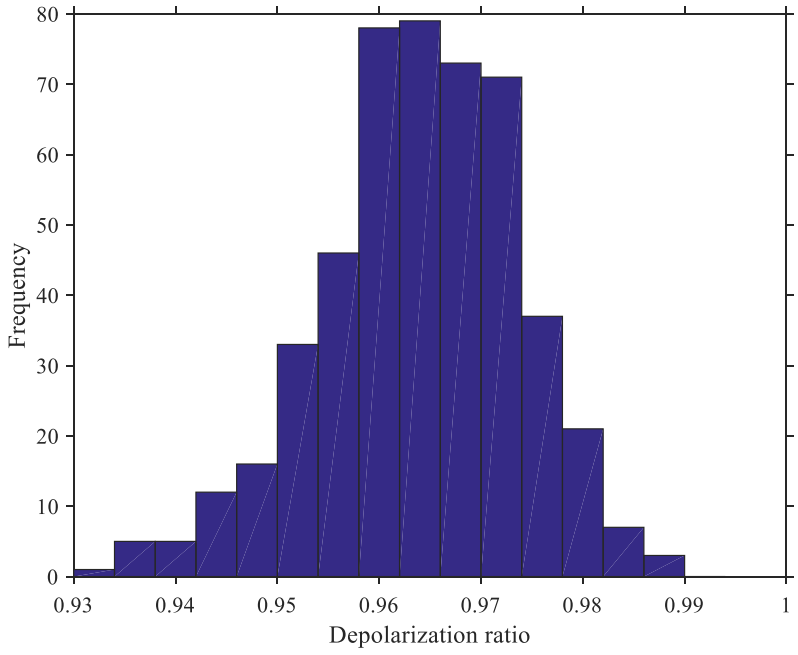

Figure 5.12 Histogram for afternoon data.

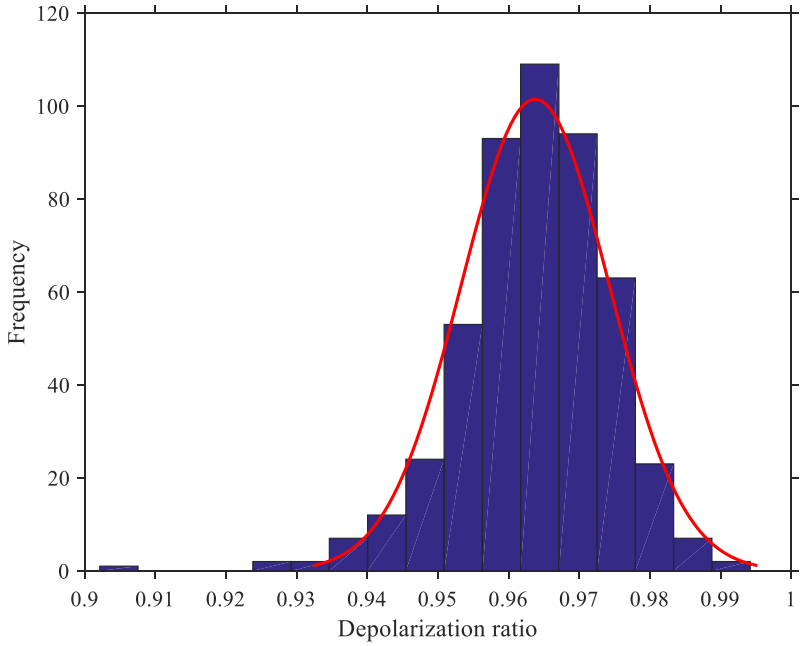

Figure 5.13 Histogram fit for afternoon data.

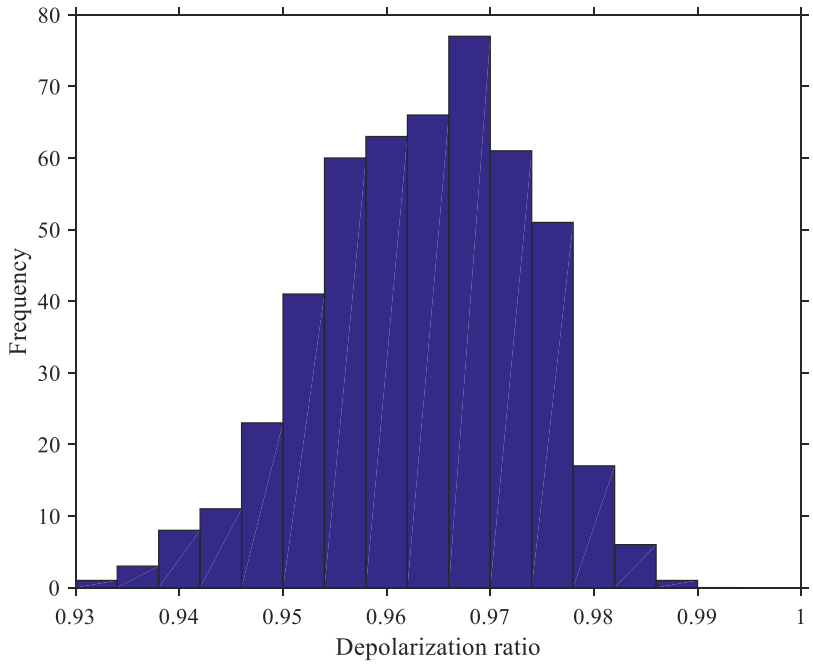

Figure 5.14 Histogram for evening data.

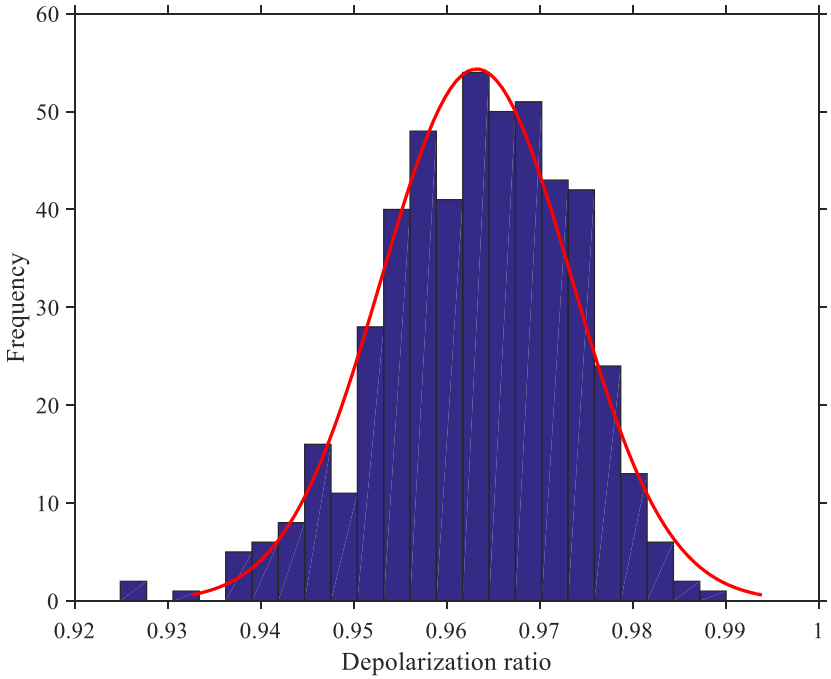

Figure 5.15 Histogram fit for evening data.

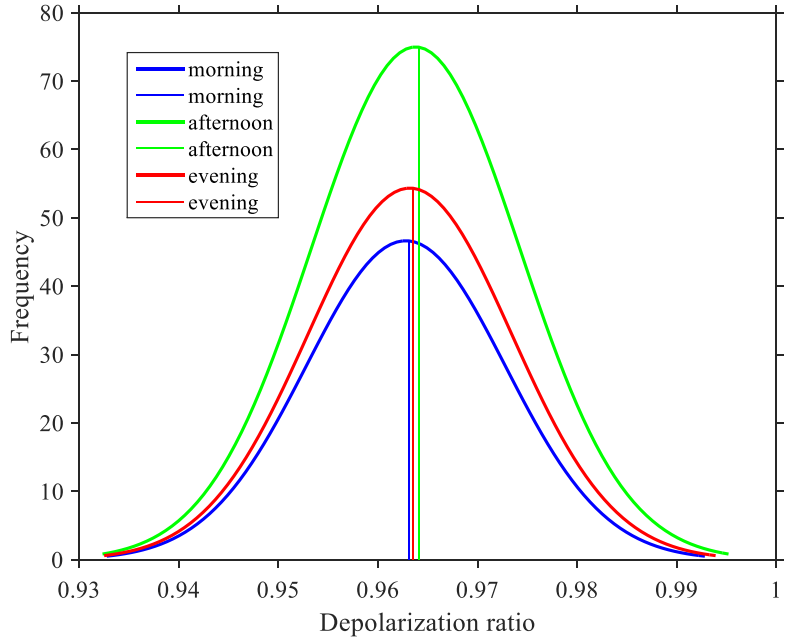

Figure 5.16 Morning, afternoon and evening histogram fit in the same graph together.

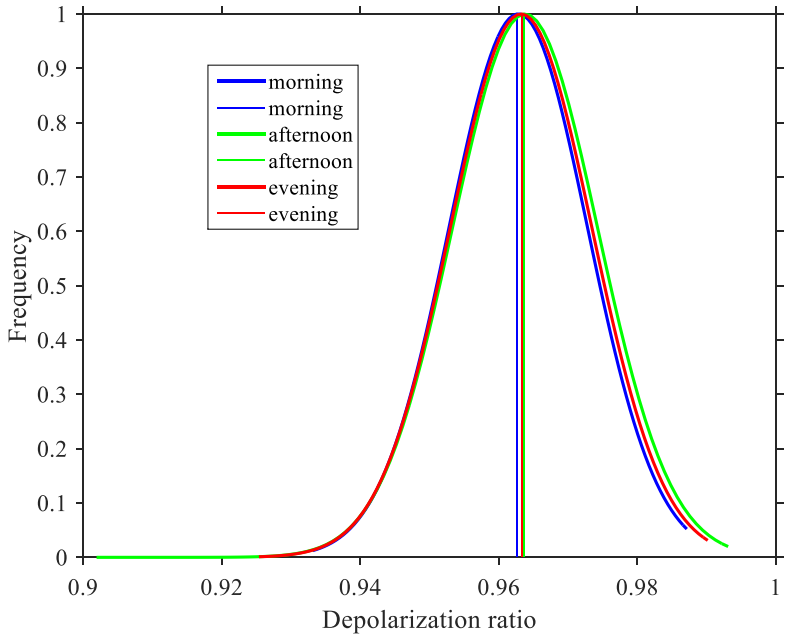

Figure 5.17 Normalized histogram fit for morning, afternoon and evening measurements in the same graph.

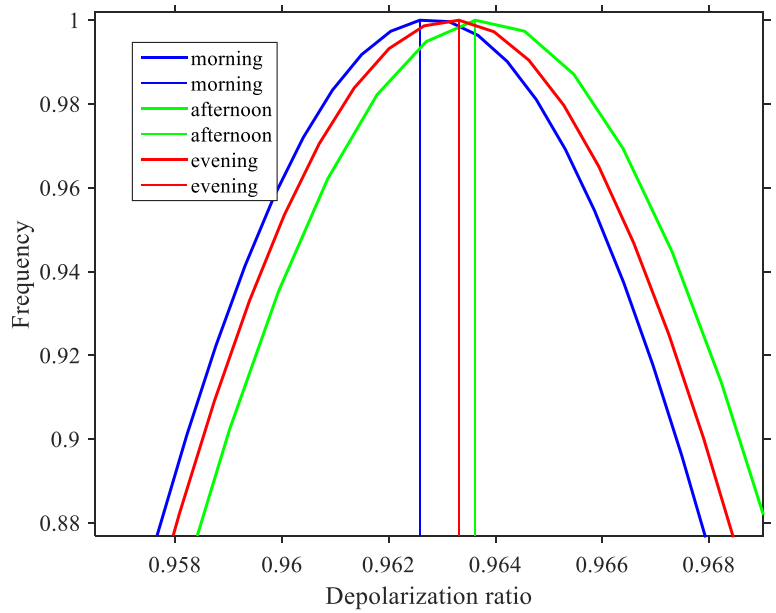

Figure 5.18 Zoomed in view of normalized histogram fit for morning, afternoon and evening measurements.

Normalized curve gives slightly different value of depolarization ratio which are 0.9626, 0.9636 and 0.9633 for morning, afternoon and evening respectively. This can be useful to visualize the change in depolarization ratio value for different times of the day. These values show how measurements executed at the different times of the day differ from each other.

Figure 5.16 to Figure 5.18 shows a shift in the distribution of the three measurements. This shift raises the possibilities that measurement done at different times of days might give the different depolarization ratio. In that case, statistical analysis is needed to see whether these datasets are different from each other or not. Statistical hypothesis testing is done in this chapter to make sure about the nature of data obtained at different times of the day.

The average value of depolarization ratio for three different times of the days are calculated directly from excel. Values calculated from excel are 0.962792, 0.963769, and 0.963201 at morning, afternoon and evening respectively. By comparing these average values calculated from excel and the depolarization ratio values corresponding to the maximum frequency on a *histfit* curve, it can be concluded that they are close enough to be considered as the same value. That means the depolarization ratio value corresponding to the maximum frequency of histogram gives an average value of the total data.

5.6 The difference in morning, afternoon and evening depolarization ratio

Even the histogram and time series plot show a slight difference in depolarization ratio for different times of the day, they should be analyzed statistically. ANOVA test was also performed to test if these three data sets were significantly different.

5.6.1 ANOVA test for three data set

One-way ANOVA test for the three different measurements was conducted using MATLAB function *anova1*. Three data sets morning, afternoon and evening were send for the ANOVA test. The null hypothesis for the ANOVA test is:

H0: means values for all the distribution is same;

An alternate hypothesis is H1: The means are not all equal.

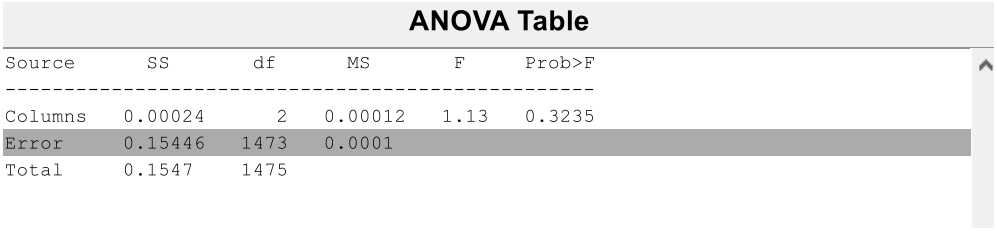

ANOVA Table

Source	SS	df	MS	F	Prob>F
Columns	0.00024	2	0.00012	1.13	0.3235
Error	0.15446	1473	0.0001		
Total	0.1547	1475			

Figure 5.19 ANOVA table for an anova1 test done on the three datasets of morning, afternoon and evening depolarization ratio.

Here the p value for the hypothesis is 0.3235 which is larger than 0.05. Function *anova1* supports the null hypothesis when the p value is greater than 0.05. Hence, there is no enough evidence to reject the hypothesis that means values for all three distributions are the same. That means we cannot say that our morning, afternoon and evening depolarization ratio value have different mean values.

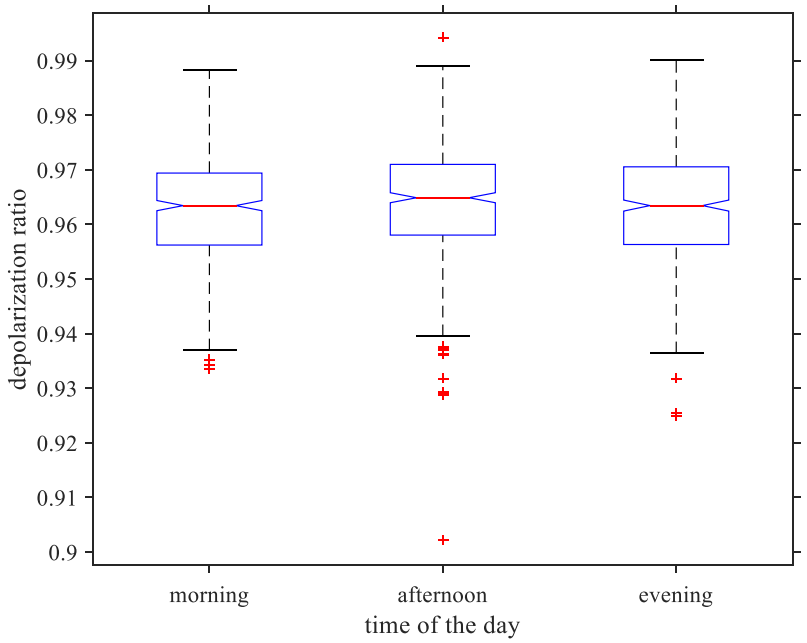

Figure 5.20 Box plot obtained from an anova1 test done on the three datasets of morning, afternoon and evening depolarization ratio.

Box plot is the visual demonstration of data distribution. Red line in box plot of Figure 5.20 shows the median of each depolarization ratio value. Minimum and maximum values on the plot are given by two horizontal lines on two ends of the box. There are few outliners in the plot also.

5.6.2 Detrending data

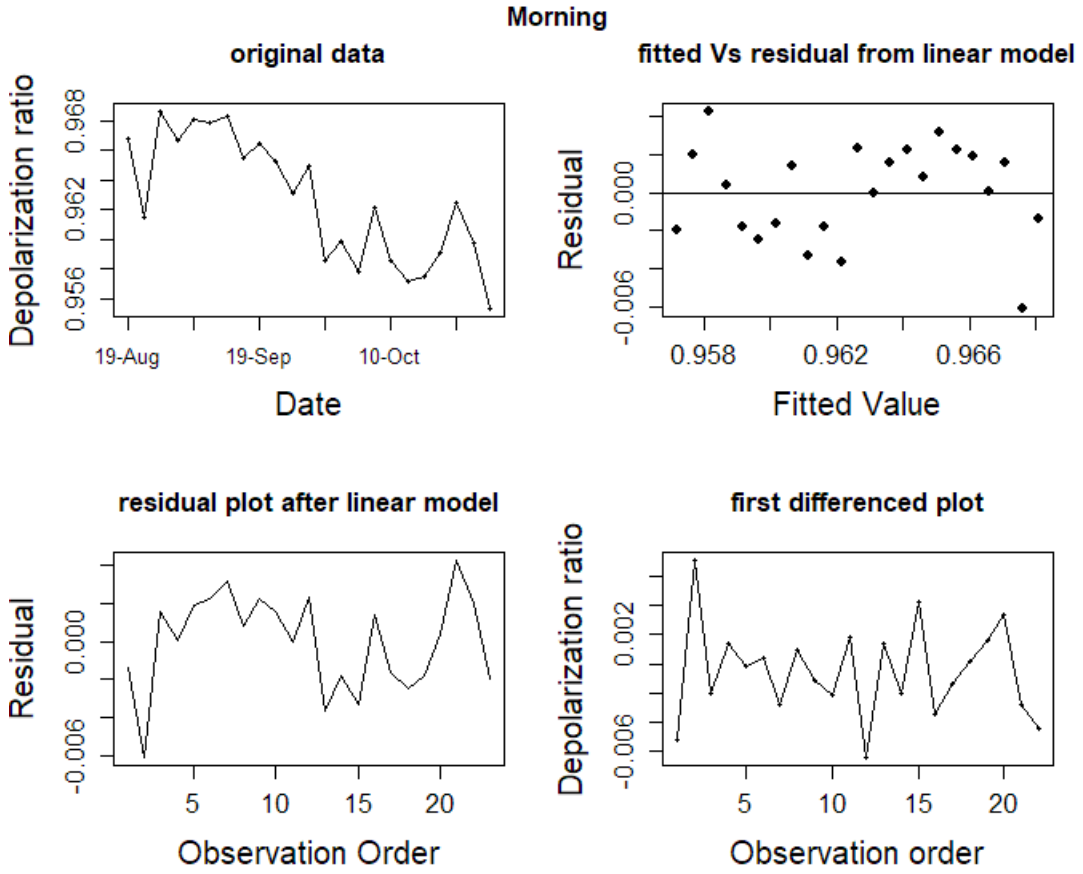

Figure 5.21 Original plot with detrended residual plot and first differenced plot of morning data.

Since the depolarization ratio value obtained from the experiment have a downward trend, detrending is desired to do the more statistical analysis. One way to detrend is to find the residual from the data doing a linear fitting. The residual obtained as below from the linear model fitting does not have a trend. Also, another way to detrend the curve is taking the first difference of data itself. The residual plot, as well as first differenced plot of all three-data series, are shown in the Figure 5.21 to Figure 5.23.

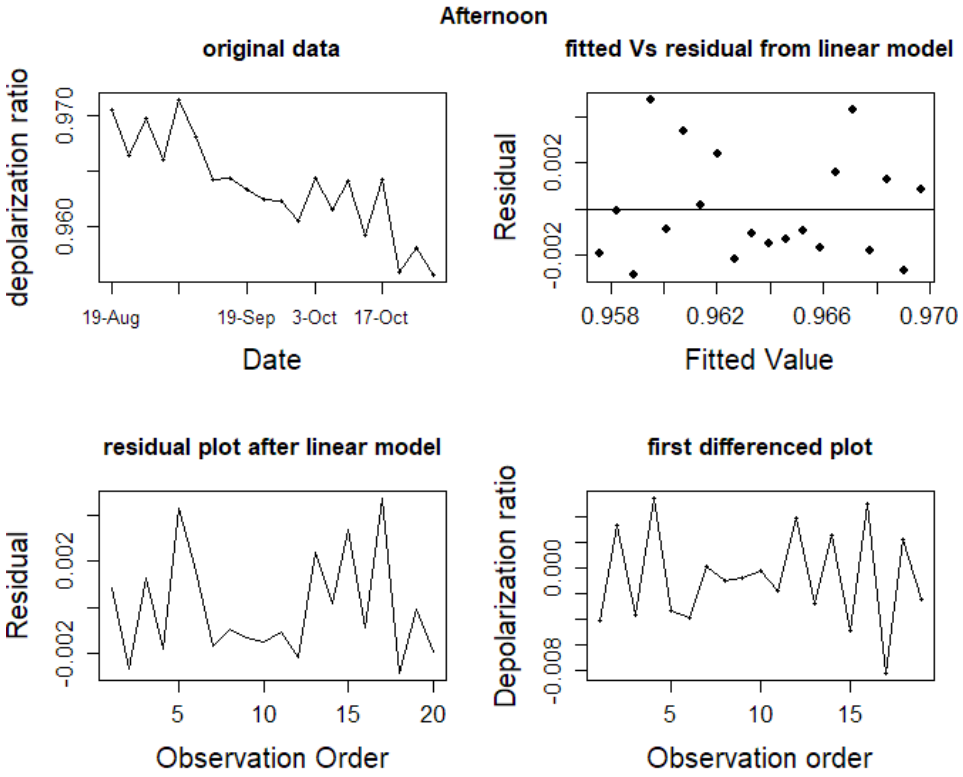

Figure 5.22 Original plot with detrended residual plot and first differenced plot of afternoon data.

5.6.2.1 ANOVA test for residual data

ANOVA test was performed on the detrended residual of three data series and analysis of variance table is shown in the Figure 5.24. The null hypothesis for the ANOVA test is:

H0: means values for all the distribution is same;

Alternate hypothesis is H1: The means are not all equal.

P value obtained was 1 which is bigger than 0.05. Hence, we cannot reject the null hypothesis. That means detrended residual also do have the same mean.

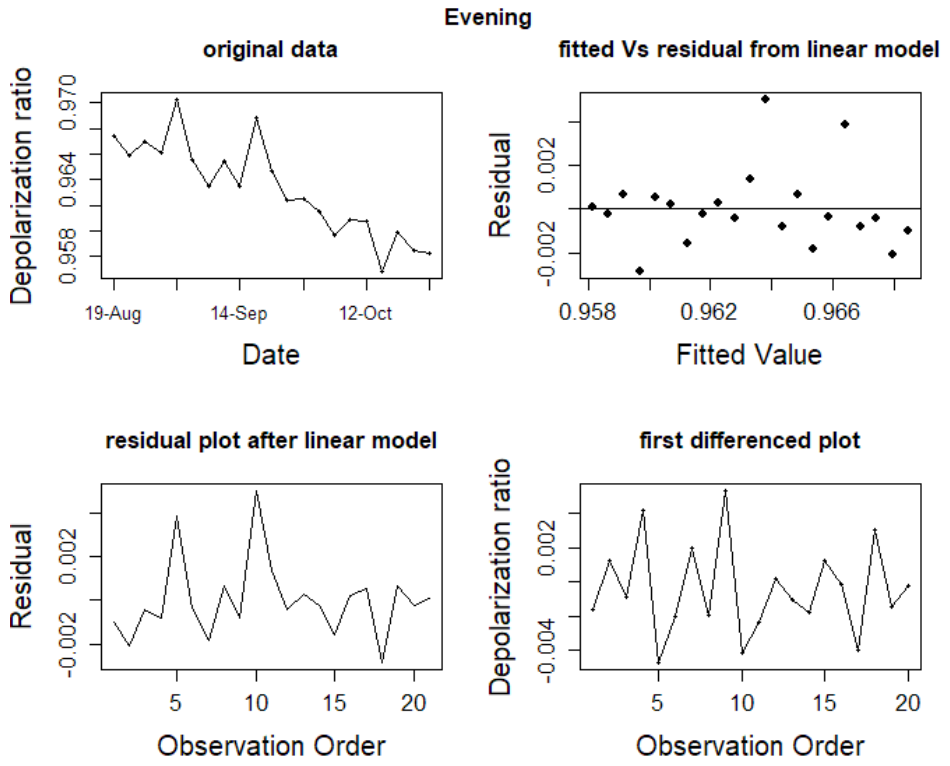

Figure 5.23 Original plot with detrended residual plot and first differenced plot of evening data.

```
> a= c(resid(morning.detrend))
> b= c(resid(afternoon.detrend))
> c= c(resid(evening.detrend))
> dati=c(a, b, c)
> groups = factor(rep(letters[1:3], c(23,20,21)))
> fit = lm(formula = dati ~ groups)
> anova(fit)
Analysis of Variance Table

Response: dati
           Df     Sum Sq    Mean Sq F value Pr(>F)
groups      2 0.00000000 0.0000e+00       0      1
Residuals 61 0.00030551 5.0083e-06
```

Figure 5.24 ANOVA test for residuals of a linear model for three series.

5.6.2.2 ANOVA test for the first differenced data set

```
Analysis of Variance Table

Response: dati
           Df     Sum Sq    Mean Sq F value Pr(>F)
groups      2 0.00000113 5.6370e-07  0.0543 0.9472
Residuals 58 0.00060195 1.0379e-05
```

Figure 5.25 ANOVA test result for the first difference of each data series.

P value for the ANOVA test of first differenced data series is also larger than 0.05. Figure 5.25 shows the analysis of variance table for the three first differenced data series. Hence null hypothesis cannot be rejected. ANOVA test for both residual and first difference of data does not support that these data series are significantly different.

5.6.2.3 T-Test after taking the difference between the two series

The difference was taken between the morning and afternoon, morning and evening, afternoon and evening by subtracting one from other. Then t-test was done for each of the difference data to see whether their mean value is zero or not. P value obtained from t-test after subtracting afternoon depolarization ratio from morning value is greater than 0.05. The t-test result is shown in the Figure 5.26. Hence, we cannot reject the null hypothesis that the mean is equal to zero. That means we cannot say that means are not equals to zero. Similarly, a t-test was done for other two differences i.e. between morning and evening as well as between afternoon and evening. In both cases, the mean value of differences cannot be considered as other than zero. T-test hence again supports that three data series are not different from each other. Although time series plot showed they are separate from each other, they were not different series in a statistical sense.

```
        One Sample t-test

data:  x
t = -0.70167, df = 15, p-value = 0.4936
alternative hypothesis: true mean is not equal to 0
95 percent confidence interval:
 -0.002892904  0.001459949
sample estimates:
    mean of x
-0.0007164774
```

Figure 5.26 T-test result after subtracting afternoon depolarization ratio from morning value.

5.7 Conclusion

All the above statistical analysis signifies that the depolarization ratio value was not significantly different at any times of the day. Hence, we can collect leaves at any times of the day for any kinds of future consideration. The important conclusion can be made regarding the downward trend line from mid-august towards the spring season. This trend can be useful to characterize the seasonal change of maple leaves and potentially useful in identifying the maple leaf from other tree plants. Moreover, this downward trend line might be the result of changing chlorophyll and other pigment conditions[46]. Since the season was going towards spring and environment was getting more drier and the plant must have been having a lot of internal changes which might affect the depolarization ratio. In the experiment, maple leaves were used which changes its color during the fall season. This change in color is related to different pigmental activities of the plant[64]. Hence this trend line is the tracking line for different kinds of internal changes happening inside the plant leaves.

CHAPTER 6 EFFECT OF WATER STRESS, RAIN, AND DEHYDRATION ON DEPOLARIZATION RATIO

6.1 Introduction

Depolarization measurement was performed in the near infrared region at 1064 nm on the foliage of maple tree which was already explained in chapter 5. The difference in pigments like chlorophyll, other biochemical composition, and water content can make a difference in the reflectance spectra[25]. After presenting the seasonal trend of depolarization ratio in an earlier chapter, this chapter is intended to investigate the effect of water stress condition in the foliage. The city of Brookings experienced few rainfalls during fall 2017. The measurement of depolarization ratio was done four times just after the rain to identify the behavior of plant leaf after rain.

6.2 Depolarization ratio measurement of maple leaf before and after the rain

The average depolarization ratio values measured before and after rainfalls are summarized in Table 6.1. For three out of four measurements done after the rain, depolarization ratio values were increased compared to the earlier measurement before rainfall. Depolarization ratio was increased in a small amount of approximately 0.004.

The overall trend of depolarization ratio in fall 2017 was downward with time. All the depolarization ratio values measured without the rain were decreasing with time. In the same sense, overall depolarization ratios measured after each rain should also be in decreasing order. However, in most of the cases, depolarization value increased after the rainfall compared with the value measured earlier just before the rainfall.

Table 6.1 Summary of depolarization ratio value before and after rain for the maple leaf.

measurement before rain			rain event			Measurement after rain		
date	Time of measurement	depolarization ratio	date of rain	Time	precipitation	date	Time of measurement	depolarization ratio
24-Aug	morning, noon, eve	0.964582	26-Aug	1 am to 3 am a night	0.1 inch	26-Aug	evening	0.967031
21-Sep	morning, noon, eve	0.964126	26-Sep	from midnight to morning	0.1inch	26-Sep	morning, noon and evening	0.962578
28-Sep	noon to evening	0.961534	30-Sep	morning	light rain	30-Sep	morning	0.96497
2-Oct	morning	0.958508	3-Oct	all night	0.51 inch	3-Oct	morning, noon and evening	0.962332

Figure 6.1 shows the depolarization ratio changes after the rainfall. The arrow heads in the figure point towards the depolarization ratio after the rainfall, starting from the corresponding value before rainfall. First rain event happened on August 26, 2017. Before that, measurement of depolarization ratio was done on August 24, 2017, and average depolarization ratio value for all the measurement was 0.964582. From 1 AM to 3 AM in the midnight of August 26, light rainfall of precipitation of 0.1 inches occurred. Then the day of 26 August was cloudy and gloomy most of the time. Average humidity was 87 and mean temperature was 68-degrees Fahrenheit. Hence when depolarization ratio value was measured during the evening of August 26, it was found to be 0.9670311.

Another rainfall happened on September 26, 2017. This time, measurement was done on 21 September and there was about a 5-day-gap for the next measurement. But before making the next measurement on 26 September, rainfall occurred. There was a rain throughout the whole night until the morning, but rain was not heavy. Precipitation was 0.1 inches and the day was mostly cloudy. This time depolarization ratio value was not increased. Depolarization ratio value of 0.964126 on 21st September had changed to 0.962578 on 26th September. Since the depolarization ratio value was measured five days ago, we cannot say depolarization ratio values does not increase after rain comparing to the before rainfall. If the value could have measured on 25th September, it could have been smaller than the value obtained at 26th. But we cannot conclude anything for the data on this date. The depolarization ratio value keeps decreasing after that date. Depolarization ratio value was measured to be 0.961534 on 28th September. The measurement was done during afternoon and evening times of 28th September. But there was again a light rain on the morning of 30th September. The whole day of 30th September was cloudy and there was

a rain during the afternoon too, but the measurement was done in the morning time only. The depolarization ratio value had increased from 0.96134 on 28th September to 0.9649695 on 30th September 2017. After September 30, there was another measurement on the 2nd of October 2017. The depolarization ratio value went down to 0.9585 on the morning of October 2nd which was lower than 30th September. But again, next rain event happened on the date of October 3 in the night before taking measurements. There was a heavy rain during the midnight of October 3 followed by light rain and overcast condition in the morning. The day was cloudy and gloomy. Hereafter the rain, depolarization ratio value went to 0.9623317. In fact, the whole measurement on 3rd October was larger than the depolarization ratio of 2nd October. During the measurement of October 3rd, leaves were still wet while they were collected in the morning. Then they were kept inside the plastic bag for around 2 hours. As seen visually, water content was not lost during that period. Then water was absorbed by the tissue paper very gently. The leaf was not damaged in the process.

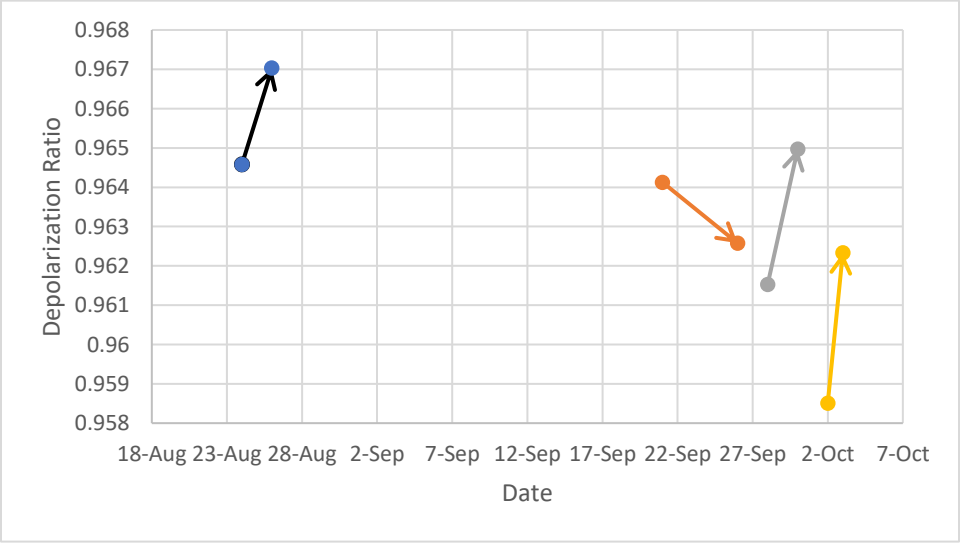

Figure 6.1 Depolarization ratio of maple tree before and after the rain denoted by aero.

6.3 Depolarization ratio for rubber tree, maple and lemon tree leaf at different water stress condition

Leaves after rainfall contain more water content in it which is believed to affect the result. So, it would be interesting to see the change in depolarization ratio value with a dry leaf too. The dry leaf is supposed to behave in opposite way than the leaf after rainfall. Although depolarization ratio after rainfall was available only for maple leaf, dry leaf depolarization ratios were measured in various other trees. Dry leaf measurement was done on a maple leaf, rubber tree leaf, and lemon tree leaf. Measurement of depolarization ratio of rubber tree after watering the tree for two weeks gave the highest value of depolarization ratio for the case of the rubber tree itself. Average depolarization ratio value was 0.936824809 with a standard deviation of 0.03154193 with high water stress. Keeping the tree without watering for 2 weeks reduced the depolarization ratio to 0.9121. 10 measurements of rubber tree were done on the same leaf. The same leaf of the same plant which was kept dry without watering for two weeks was measured again. The same watering and drying process yield a depolarization ratio trend as shown in Figure 6.2. In addition, maple leaves were collected and measured while they were still fresh. Then the leaves were kept in the lab and let to be dried. In the similar fashion, A lemon leaf was collected, and the depolarization ratio was measured for the fresh leaf. Then the leaf was kept on the lab and continued measuring the depolarization ratio value as it dried. The measured average result is summarized in Table 6.2 to Table 6.4.

Table 6.2 Depolarization ratio summary for drying rubber tree leaves.

	Leaf 1		Leaf2	
Date	STD	AVG	STD	AVG
10/22/2017	0.030242	0.93256		
11/5/2017	0.019829	0.912146		
11/9/2017	0.023679	0.914323		
11/24/2017			0.029014	0.921882
11/28/2017			0.023961	0.900514
11/30/2017			0.049526	0.901716
12/10/2017			0.032964	0.895525
12/14/2017			0.007177	0.893185

Table 6.3 Depolarization ratio summary for drying maple tree leaves.

	Leaf1		Leaf2		Leaf 3	
Date	STD	AVG	STD	AVG	STD	AVG
9/28/2017	0.008264	0.962427			0.005431	0.958617
10/5/2017			0.009861	0.95737		
11/2/2017	0.009928	0.950049			0.009143	0.955653
11/7/2017	0.00898	0.941066	0.014223	0.955104		
11/14/2017	0.012195	0.941782				
11/16.2017			0.010629	0.950343		

Table 6.4 Depolarization ratio summary for drying lemon tree leaves.

	Leaf1		Leaf2		Leaf3		Leaf4	
Date	STD	AVG	STD	AVG	STD	AVG	STD	AVG
10/31/2017					0.0116	0.9479		
11/7/2017			0.0095	0.9606	0.0184	0.941		
11/9/2017			0.0235	0.9533	0.009	0.9388		
11/14/2017	0.0098	0.9596	0.0142	0.9534	0.0107	0.9450		
11/16/2017	0.0068	0.9431	0.0103	0.9542	0.0083	0.9387		
11/18/2017	0.0128	0.9401						
11/21/2017	0.0089	0.9507	0.0079	0.9545			0.0053	0.9487
11/23/2017	0.0091	0.9422					0.0071	0.9454
11/24/2017					0.0105	0.9427		
11/28/2017	0.009	0.9401					0.0052	0.9405
11/30/2017					0.0063	0.9412	0.0103	0.9423
12/14/2017							0.0048	0.9435

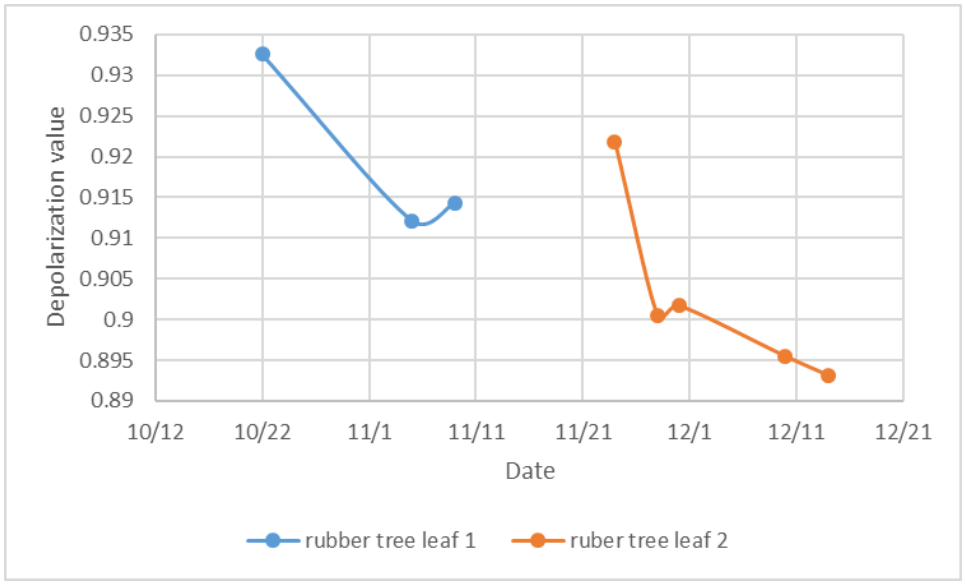

Figure 6.2 Depolarization ratio of rubber tree with time with drying condition.

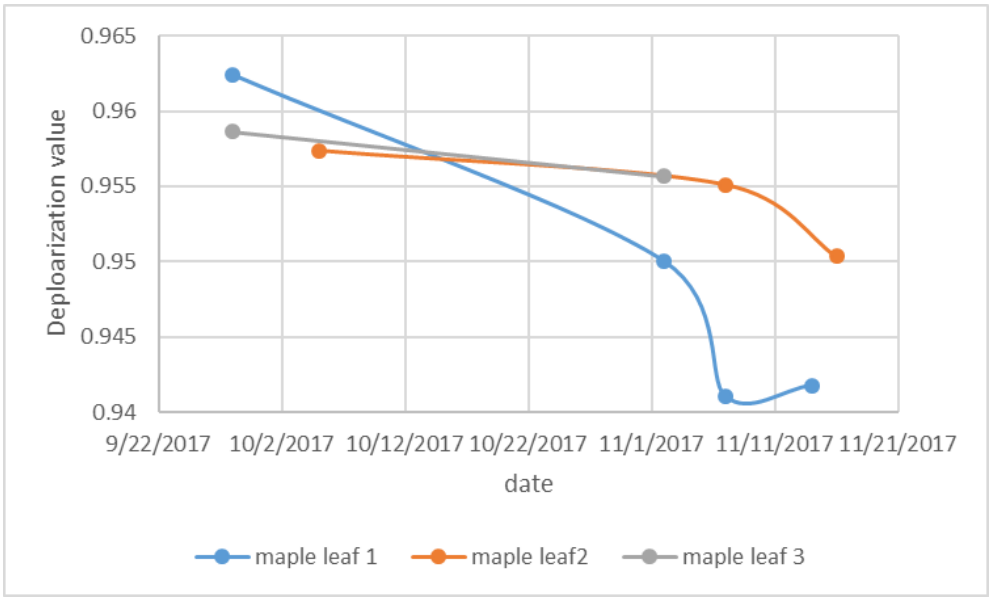

Figure 6.3 Depolarization ratio of maple leaf with time with drying condition.

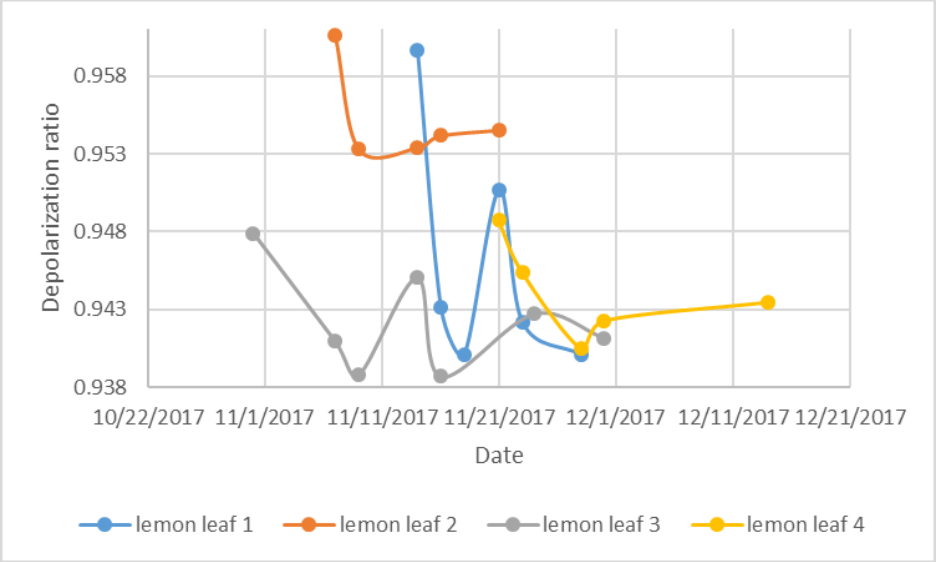

Figure 6.4 Depolarization ratio of the lemon leaf with time with drying condition.

Each data points in the graph or table above are the averages of 6 to 10 measurements on each leaf. The overall trend of the depolarization ratio of the leaf upon dry condition was downward with time. The more dried the leaf was, the smaller the depolarization ratio value became. But this decreasing trend stopped after a certain time, presumably when the leaves had lost most water.

Furthermore, from observation of depolarization ratios of three different trees, the range of depolarization was found to be different from each other. Rubber tree had the range of depolarization value from around 0.93 to 0.89. But for both maple and lemon, depolarization value fall in the range above 0.94. This difference in the range along with variation in the slope of trendline make it possible to differentiate one tree from other.

6.4 Conclusion

The observation of depolarization ratio after rain and after dehydration reveals that the depolarization ratio has a downward trend with dryness. In the case of a maple leaf, the

ratio goes up on rain and drops down on dryness. In the case of the rubber tree and lemon tree, dryness with time decreases the depolarization ratio to a certain point and then stays almost flat. Also, the trend and range of depolarization value were different from each other.

CHAPTER 7 CONCLUSIONS

7.1 Contributions

There are many issues in the forest and plant management. For instance, the native tree species are attacked by the invasive species in some forests. This may affect the forest ecological environment. In other places, some of the plants are dying due to diseases; and this is affecting the ecological balance. A forest fire is another important issue that causes huge damage to the human society. Remote sensing techniques can help us to study on these issues and figure out ways to prevent them from happening. This thesis research has the following important contributions in plant and vegetation remote sensing:

1. This is the first reported research which demonstrates that polarimetric lidar sensor at the near-infrared wavelength is sensitive enough to identify the internal changes happening inside the plant. This is a very important ability of the polarimetric lidar.

2. This research reveals that the polarimetric lidar can detect the water stress condition of plants. This is an effective way to monitor vegetation water stress and assess forest fire hazard from a remote place. Tracking the water stress of plant is very important to assess and predict fire hazard in the forest.

3. In this thesis, the polarimetric lidar is used to characterize the seasonal change of plant leaves by monitoring its polarimetric behavior. This work has been successful in showing the seasonal change of the maple tree leaves.

4. This research points out that the polarimetric lidar can also be used to identify plant species. Unlike passive remote sensing, this identification process can work during night time.

7.2 Conclusions

This study uses a novel approach to find out the changes of plant leaves using the polarization property of laser. In the study of seasonal behavior on maple leaves, a decreasing depolarization trend was observed. The downward trend is interesting and suggests that the lidar is able to characterize the internal changes happening in the maple leaves. Therefore, the biological and physiological change in plant throughout the season may also be characterized using this method. Through statistical analysis, it is discovered that there is not a significant difference in the diurnal change of the depolarization value. So that measurement done at any times of the day would not affect the seasonal trend.

Four rain events happened during the study of the maple tree leaves. The depolarization ratios measured right after the rain give larger ratio values. Since the overall seasonal trend is in a downward direction, the after-rain values should get smaller instead of larger. This larger depolarization after rain suggests that the rain falls contributes to the depolarization change. Further study shows that the depolarization ratio goes down when the leaves are dried. Drying depolarization ratio was tested for maple, lemon and rubber tree leaves. In all three tree leaves, the trend was downward after drying. This demonstrates that the laser sensor is able to sense the water content change in plant leaves.

In addition, the range of the depolarization ratio value differs from each other; and the trend line differs from each other too. This can help to differentiate one plant from the others using the polarimetric lidar.

In conclusion, this study reveals that the polarimetric lidar sensor is a very useful tool for vegetation remote sensing. Tracking the changes happening in the leaves throughout a season was not achieved by a lidar before. This study opens a door for the

vegetation remote sensing that can measure both the external features and the internal features of the plants.

7.3 Limitations and future work

The experiment was done in fall of 2017 and the seasonal study was done only on the maple leaves. Data from only one season were collected, the multiple-season study is needed to fully characterize the annul behavior of plant leaves. In order to more accurately characterize the trend line for any specific plant, the measurement should be done for multiple years to improve the signal-to-noise ratio of the data. In addition, a comparative study on more tree species is needed. This will help to develop the classification algorithms for different tree species using polarimetric lidar.

In the case of leaf dehydration and rain event measurement, more samples can be used. Leaves can be soaked and weighted, so the leaf water content can be quantified. Weight measurement will provide an accurate measure of the water loss or increase of the leaf. This will lead to a quantitative description of the effect of water on the depolarization ratio.

Another improvement of the experiment that can be done is to measure the biological parameters. Biological parameters such as chlorophyll and other pigments, or nitrogen contents, etc. can be obtained before the measurement of the depolarization ratio. Measuring these biological parameters will provide more insight into the understanding of the reasons for the change of depolarization value.

All our experiments were performed inside a dark room. Leaves were collected in the field and measured in the lab. On site measurement of the leaves in the field is needed

for practical applications. Leaves detached from a tree may experience changes compared with these still on the tree. Instead of drying the leaf in the lab, the measurement can be done when leaves become dry on the tree. Nevertheless, improving the lab-based polarimetric lidar system is important to the application of this lidar technology in the future, which will improve our capability in vegetation remote sensing.

REFERENCES

[1] Hamamatsu Photonics. *History of research on the light*. Available: http://photonterrace.net/en/photon/history/

[2] Clean Enery Institute University of Washington. *Double Refraction and Birefringence*. Available: http://photonicswiki.org/index.php?title=Double_Refraction_and_Birefringence

[3] J. D. Mollon, "The origins of the concept of interference," (in eng), *Philos Trans A Math Phys Eng Sci*, vol. 360, no. 1794, pp. 807- 2002.

[4] Environmental Optics Laboratory (Eötvös University). *Brief History of the Discovery of Phenomena Concerning Light Polarization*. Available: https://arago.elte.hu/sites/default/files/DSc-Thesis-2003-GaborHorvath-01.pdf

[5] W. M. Boerner, H. Mott, and E. Luneburg, "Polarimetry in remote sensing: basic and applied concepts," in *Geoscience and Remote Sensing, 1997. IGARSS '97. Remote Sensing - A Scientific Vision for Sustainable Development., 1997 IEEE International*, vol. 3, pp. 1401-1403 vol.3. 1997

[6] Physics Classroom. *Polarization*. Available: http://www.physicsclassroom.com/class/light/Lesson-1/Polarization

[7] A. Wehr and U. Lohr, "Airborne laser scanning—an introduction and overview," *ISPRS Journal of Photogrammetry and Remote Sensing*, vol. 54, no. 2, pp. 68-82, 1999.

[8] J. Carter *et al.* (2012). *Lidar 101: An Introduction to Lidar Technology, Data, and Applications*. Available: https://coast.noaa.gov/data/digitalcoast/pdf/lidar-101.pdf

[9] M. A. Lefsky, D. Harding, W. B. Cohen, G. Parker, and H. H. Shugart, "Surface Lidar Remote Sensing of Basal Area and Biomass in Deciduous Forests of Eastern Maryland, USA," *Remote Sensing of Environment,* vol. 67, no. 1, pp. 83-98, 1999.

[10] J. B. Blair, D. L. Rabine, and M. A. Hofton, "The Laser Vegetation Imaging Sensor: a medium-altitude, digitisation-only, airborne laser altimeter for mapping vegetation and topography," *ISPRS Journal of Photogrammetry and Remote Sensing,* vol. 54, no. 2, pp. 115-122, 1999.

[11] D. B. Coyle, R. B. Kay, and S. J. Lindauer, "Design and performance of the vegetation canopy Lidar (VCL) laser transmitter," in *Proceedings, IEEE Aerospace Conference*vol. 3, pp. 3-1457-3-1464 vol.3. 2002

[12] S. Tan, R. M. Narayanan, and D. L. Helder, "Polarimetric reflectance and depolarization ratio from several tree species using a multiwavelength polarimetric lidar," in SPIE *Optics and Photonics 2005,*vol. 5888, p. 9: 2005

[13] P. S. Argall and R. J. Sica, "Lidar," *The University of Western Ontario, London,Ontario,Canada,* pp. 869-889, 2002.

[14] L. A. Wasser. *The Basics of LiDAR - Light Detection and Ranging - Remote Sensing*. Available: http://www.neonscience.org/lidar-basics

[15] J. Z. Zhu, Z., Hu, X., Li, Z., "ANALYSIS AND APPLICATION OF LIDAR WAVEFORM DATA USING A PROGRESSIVE WAVEFORM DECOMPOSITION METHOD," *Int. Arch. Photogramm. Remote Sens. Spatial Inf. Sci.*, vol. XXXVIII-5/W12, no. 31,36, . Copernicus Publications, 2012

[16] K. D. Fieber, I. J. Davenport, J. M. Ferryman, R. J. Gurney, J. P. Walker, and J. M. Hacker, "Analysis of full-waveform LiDAR data for classification of an orange

orchard scene," *ISPRS Journal of Photogrammetry and Remote Sensing*, vol. 82, pp. 63-82, 2013.

[17] B. Höfle and N. Pfeifer, "Correction of laser scanning intensity data: Data and model-driven approaches," *ISPRS Journal of Photogrammetry and Remote Sensing*, vol. 62, no. 6, pp. 415-433, 2007.

[18] J. Rosette, C. Field, R. Nelson, P. Decola, and B. Cook, *A new photon-counting lidar system for vegetation analysis*. 2011.

[19] L. Marchese, S. Turbide, M. Terroux, and A. Bergeron, "All optical Synthetic Aperture Lidar sensing-to-processing chain based on SAR technology," *IEEE International Geoscience and Remote Sensing Symposium*, pp. 5006-5008. 2012.

[20] G. Vane and A. F. H. Goetz, "Terrestrial imaging spectroscopy," *Remote Sensing of Environment*, vol. 24, no. 1, pp. 1-29, 1988.

[21] Jet Propulsion Laboratory California Institute of Technology. *AVIRIS Overview*. Available: https://aviris.jpl.nasa.gov/aviris/index.html

[22] A. F. H. Goetz, "The Portable Instant Display and Analysis Spectrometer (PIDAS),". Conference Paper. 1987

[23] T. Key, T. Warner, J. McGraw, and M.A. Fajvan, "A comparison of multispectral and multitemporal imagery for tree species classification," *Remote Sensing of Environment*, vol. 75, pp. 100-112, 2001.

[24] A. Burkholder, T. A. Warner, M. Culp, and R. Landenberger, "Seasonal Trends in Separability of Leaf Reflectance Spectra for Ailanthus altissima and Four Other Tree Species," *Photogrammetric Engineering & Remote Sensing*, vol. 77, pp. 793-804, August 2011.

[25] G. P. Asner, M. O. Jones, R. E. Martin, D. E. Knapp, and R. F. Hughes, "Remote sensing of native and invasive species in Hawaiian forests," *Remote Sensing of Environment*, vol. 112, no. 5, pp. 1912-1926, 2008.

[26] B. Somers and G. P. Asner, "Hyperspectral Time Series Analysis of Native and Invasive Species in Hawaiian Rainforests," *Remote Sensing*, vol. 4, no. 9, 2012.

[27] M. Voss and R. Sugumaran, "Seasonal Effect on Tree Species Classification in an Urban Environment Using Hyperspectral Data, LiDAR, and an Object-Oriented Approach," *Sensors (Basel, Switzerland)*, vol. 8, no. 5, pp. 3020-3036, 2008.

[28] T. Brandtberg, T. Warner, R. Landenberger, and J. McGraw, *Detection and analysis of individual leaf-off tree crowns in a small footprint, high sampling density lidar data from the eastern deciduous forest in North America*., pp. 290-303. 2003

[29] E. Næsset, "Determination of mean tree height of forest stands using airborne laser scanner data," *ISPRS Journal of Photogrammetry and Remote Sensing*, vol. 52, no. 2, pp. 49-56, 1997.

[30] S. C. Popescu, R. H. Wynne, and R. F. Nelson, "Estimating plot-level tree heights with lidar: local filtering with a canopy-height based variable window size," *Computers and Electronics in Agriculture*, vol. 37, no. 1-3, pp. 71-95, 2002.

[31] M. L. Clark, D. B. Clark, and D. A. Roberts, "Small-footprint lidar estimation of sub-canopy elevation and tree height in a tropical rain forest landscape," *Remote Sensing of Environment*, vol. 91, no. 1, pp. 68-89, 2004.

[32] E. Næsset and T. Gobakken, *Estimating forest growth using canopy metrics derived from airborne laser scanner data*., pp. 453-465. 2005.

[33] S. D. Roberts, T. J. Dean, D. L. Evans, J. W. McCombs, R. L. Harrington, and P. A. Glass, "Estimating individual tree leaf area in loblolly pine plantations using LiDAR-derived measurments of height and crown dimensions,", Available: https://www.fs.usda.gov/treesearch/pubs/20903. 2005.

[34] S. Solberg, E. Næsset, and O. Martin Bollandsas, *Single Tree Segmentation Using Airborne Laser Scanner Data in a Structurally Heterogeneous Spruce Forest*., pp. 1369-1378. 2006.

[35] Z. J. Bortolot, "Using Tree Clusters to Derive Forest Properties from Small Footprint Lidar Data," *Photogrammetric Engineering & Remote Sensing*, vol. 72, no. 12, pp. 1389-1397, 2006.

[36] E. S. Rowell, Carl; Vierling, Lee; Queen, Lloyd; Sheppard, Wayne., "Using laser altimetry-based segmentation to refine automated tree identification in managed forests of the Black Hills, South Dakota," *Photogrammetric Engineering and Remote Sensing*, vol. 72, no. 2, pp. 1379-1388, 2006.

[37] L. Cao, N. Coops, T. Hermosilla, J. Innes, J. Dai, and G. She, "Using Small-Footprint Discrete and Full-Waveform Airborne LiDAR Metrics to Estimate Total Biomass and Biomass Components in Subtropical Forests," *Remote Sensing*, vol. 6, no. 8, p. 7110, 2014.

[38] P. K. J. Reitberger, U. Stilla, "Combined Tree Segmentation and Stem Detection Using Full Waveform Lidar Data," *Conference Proceedings*, 2007.

[39] J. Reitberger, P. Krzystek, and U. Stilla, "Analysis of full waveform LIDAR data for the classification of deciduous and coniferous trees," *International Journal of Remote Sensing*, vol. 29, no. 5, pp. 1407-1431, 2008.

[40] C. Mallet and F. Bretar, *Full-waveform topographic lidar: State-of-the-art*., pp. 1-16. 2009.

[41] D. S. Kimes, K. J. Ranson, G. Sun, and J. B. Blair, "Predicting lidar measured forest vertical structure from multi-angle spectral data," *Remote Sensing of Environment*, vol. 100, no. 4, pp. 503-511, 2006.

[42] D. J. Harding, M. A. Lefsky, G. G. Parker, and J. B. Blair, "Laser altimeter canopy height profiles: methods and validation for closed-canopy, broadleaf forests," *Remote Sensing of Environment*, vol. 76, no. 3, pp. 283-297, 2001.

[43] M. Königer, G. C. Harris, and E. Kibler, "Seasonal changes in the physiology of shade leaves of Acer saccharum," *Journal of Plant Physiology*, vol. 157, no. 6, pp. 627-636, 2000.

[44] G. P. Asner, C. A. Wessman, C. A. Bateson, and J. L. Privette, "Impact of Tissue, Canopy, and Landscape Factors on the Hyperspectral Reflectance Variability of Arid Ecosystems," *Remote Sensing of Environment*, vol. 74, no. 1, pp. 69-84, 2000.

[45] B. Kötz, M. Schaepman, F. Morsdorf, P. Bowyer, K. Itten, and B. Allgöwer, "Radiative transfer modeling within a heterogeneous canopy for estimation of forest fire fuel properties," *Remote Sensing of Environment*, vol. 92, no. 3, pp. 332-344, 2004.

[46] F. Morsdorf, C. Nichol, T. Malthus, and I. H. Woodhouse, "Assessing forest structural and physiological information content of multi-spectral LiDAR waveforms by radiative transfer modelling," *Remote Sensing of Environment*, vol. 113, no. 10, pp. 2152-2163, 2009.

[47] B. Koetz *et al.*, "Fusion of imaging spectrometer and LIDAR data over combined radiative transfer models for forest canopy characterization," *Remote Sensing of Environment*, vol. 106, no. 4, pp. 449-459, 2007.

[48] K. Sassen, "The Polarization Lidar Technique for Cloud Research: A Review and Current Assessment," *Bulletin of the American Meteorological Society*, vol. 72, no. 12, pp. 1848-1866, 1991.

[49] S. N. Volkov, I. V. Samokhvalov, H. D. Cheong, and D. Kim, "Investigation of East Asian clouds with polarization light detection and ranging," *Applied Optics*, vol. 54, no. 11, pp. 3095-3105, 2015.

[50] W.-N. Chen, C.-W. Chiang, and J.-B. Nee, "Lidar ratio and depolarization ratio for cirrus clouds," *Applied Optics*, vol. 41, no. 30, pp. 6470-6476, 2002.

[51] J. Cariou, B. Le Jeune, J. Lotrian, and Y. Guern, "Polarization effects of seawater and underwater targets," *Applied Optics*, vol. 29, no. 11, pp. 1689-1695, 1990.

[52] L. J. Mullen, A. J. C. Vieira, P. R. Herezfeld, and V. M. Contarino, "Application of RADAR technology to aerial LIDAR systems for enhancement of shallow underwater target detection," *IEEE Transactions on Microwave Theory and Techniques*, vol. 43, no. 9, pp. 2370-2377, 1995.

[53] J. E. Kalshoven and P. W. Dabney, "Remote sensing of the Earth's surface with an airborne polarized laser," *IEEE Transactions on Geoscience and Remote Sensing*, vol. 31, no. 2, pp. 438-446, 1993.

[54] S. Tan and J. Stoker, "Multiwavelength Polarimetric Lidar for Foliage Obscured Man-Made Target Detection," in *Advances in Geoscience and Remote Sensing*, G. Jedlovec, Ed. Rijeka: InTech, p. Ch. 18. 2009.

[55] Edmund Optics. *Rotary Optic Mount*. Available: https://www.edmundoptics.com/optomechanics/optical-mounts/polarizer-mounts/rotary-optic-mount/#resources

[56] C. J. Tucker and M. W. Garratt, "Leaf optical system modeled as a stochastic process," *Applied Optics,* vol. 16, no. 3, pp. 635-642, 1977.

[57] M. Qinglin, A. Ishimaru, P. Phu, and Y. Kuga, "Transmission, reflection, and depolarization of an optical wave for a single leaf," *IEEE Transactions on Geoscience and Remote Sensing,* vol. 28, no. 5, pp. 865-872, 1990.

[58] V. C. Vanderbilt, L. Grant, and C. S. T. Daughtry, "Polarization of light scattered by vegetation," *Proceedings of the IEEE,* vol. 73, no. 6, pp. 1012-1024, 1985.

[59] T. R. Sinclair, M. M. Schreiber, and R. M. Hoffer, *Diffuse Reflectance Hypothesis for the Pathway of Solar Radiation Through Leaves1*.Agron. J. 65:276-283,1973.

[60] physics.stackexchange.com. Available: https://physics.stackexchange.com/questions/359696/how-do-electromagnetic-waves-wave

[61] emedicalprep.com. Available: https://www.emedicalprep.com/study-material/physics/wave-optics/polarization/

[62] Electronics Hub. *Circular polarization*. Available: https://www.electronicshub.org/electromagnetic-waves/

[63] kristoflodewijks.be. *Spectroscopic Ellipsometry*. Available: http://www.kristoflodewijks.be/?page_id=262

[64] H. Yang, X. Yang, M. Heskel, S. Sun, and J. Tang, "Seasonal variations of leaf and canopy properties tracked by ground-based NDVI imagery in a temperate forest," *Scientific Reports*, vol. 7, no. 1, p. 1267, 2017.